

See discussions, stats, and author profiles for this publication at: <https://www.researchgate.net/publication/51642447>

# Nonresonant and Resonant Mode-Specific Intermolecular Vibrational Energy Transfers in Electrolyte Aqueous Solutions

ARTICLE in THE JOURNAL OF PHYSICAL CHEMISTRY A · SEPTEMBER 2011

Impact Factor: 2.69 · DOI: 10.1021/jp206937u · Source: PubMed

---

CITATIONS

26

---

READS

22

## 5 AUTHORS, INCLUDING:



Hailong Chen

Rice University

23 PUBLICATIONS 267 CITATIONS

[SEE PROFILE](#)



Jiebo Li

Rice University

24 PUBLICATIONS 357 CITATIONS

[SEE PROFILE](#)



Junrong Zheng

Rice University

52 PUBLICATIONS 1,529 CITATIONS

[SEE PROFILE](#)

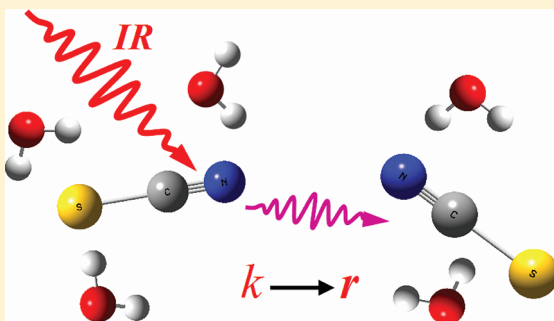
# Nonresonant and Resonant Mode-Specific Intermolecular Vibrational Energy Transfers in Electrolyte Aqueous Solutions

Hongtao Bian, Hailong Chen, Jiebo Li, Xiewen Wen, and Junrong Zheng\*

Department of Chemistry, Rice University, Houston, Texas 77005, United States

Supporting Information

**ABSTRACT:** The donor/acceptor energy mismatch and vibrational coupling strength dependences of interionic vibrational energy transfer kinetics in electrolyte aqueous solutions were investigated with ultrafast multiple-dimensional vibrational spectroscopy. An analytical equation derived from the Fermi's Golden rule that correlates molecular structural parameters and vibrational energy transfer kinetics was found to be able to describe the intermolecular mode specific vibrational energy transfer. Under the assumption of the dipole–dipole approximation, the distance between anions in the aqueous solutions was obtained from the vibrational energy transfer measurements, confirmed with measurements on the corresponding crystalline samples. The result demonstrates that the mode-specific vibrational energy transfer method holds promise as an angstrom molecular ruler.



## 1. INTRODUCTION

Electrolyte aqueous solutions are important in chemistry, biology, and atmospheric environment sciences. The dynamics of water around cations and anions and the specific ion effects on the hydrogen bonding network of water are under intense experimental and theoretical studies.<sup>1–10</sup> However, about the ion–ion interactions, especially whether ions form ion pairs or ion clusters in aqueous solutions is still a lack of consensus at the microscopic molecular level.<sup>11</sup>

The ion–ion, ion–solvent, and ion–biomolecule interactions in aqueous solutions are typically within 1 nm.<sup>12</sup> Such a short distance cannot be investigated by the FRET method because of the big sizes of labeling dye molecules (typically >1 nm).<sup>13</sup> The mode specific vibrational energy transfer method using chemical bonds themselves as energy donors and acceptors has potential to address this issue.<sup>14,15</sup> We recently demonstrated that, under the dipole–dipole approximation, the short-range interanion distance ( $\sim 0.4$  nm) in the KSCN ion clusters in medium and concentrated KSCN aqueous solutions could be estimated with the mode specific vibrational energy transfer method.<sup>3</sup> The initial demonstration is exciting and seems promising. However, there are still many fundamental questions waiting for answers before this method can be applied to general studies of transient or static short-range molecular distances in condensed phases: (1) First of all, how are the vibrational energy transfer kinetics quantitatively associated with molecular structural parameters, for example, the energy donor/acceptor coupling strength, the donor/acceptor energy mismatch, and the environment? (2) The chemical bond length (0.1–0.2 nm) and the donor/acceptor distance (0.2–1 nm) are at the same length scale. How are the starting and ending points of the distance reliably defined? (3) The experimentally

measured distance is the distance between two transition dipole moments. How is this distance quantitatively converted into the bond distance? (4) Many other interactions, e.g. mechanical couplings or high order interactions, can also play roles. These interactions have different expressions for the coupling strength. How can one interaction be distinguished from another? In this work, we are focused on answering the first question.

We have recently investigated intermolecular vibrational energy transfers in several systems.<sup>14–16</sup> From these experiments,<sup>14,15</sup> we found that an analytical equation derived from the Fermi's Golden rule which correlates molecular structural parameters and vibrational energy transfer kinetics was able to describe the intermolecular mode specific vibrational energy transfers in two very different systems:<sup>15</sup>

$$k_{ij} = \frac{1}{1 + \exp\left(-\frac{\hbar\omega_{ij}}{kT}\right)} \times \langle\beta\rangle^2 \times \frac{\tau_c^{-1}}{\tau_c^{-2} + \omega_{ij}^2} \quad (1)$$

where  $\omega_{ij}$  is the energy mismatch between the donor and acceptor modes  $i$  and  $j$ .  $\langle\beta\rangle$  is the average coupling strength between  $i$  and  $j$ .  $\tau_c$  is the coupling correlation time. Predictions from eq 1 fit two previously investigated systems reasonably well.<sup>14</sup> However, there are three parameters in eq 1. The dependence of  $k_{ij}$  on each parameter has not been experimentally independently investigated. It is not clear whether the consistency between the predictions and the results from two previous systems is real or just coincident.

**Received:** July 20, 2011

**Revised:** September 13, 2011

**Published:** September 14, 2011

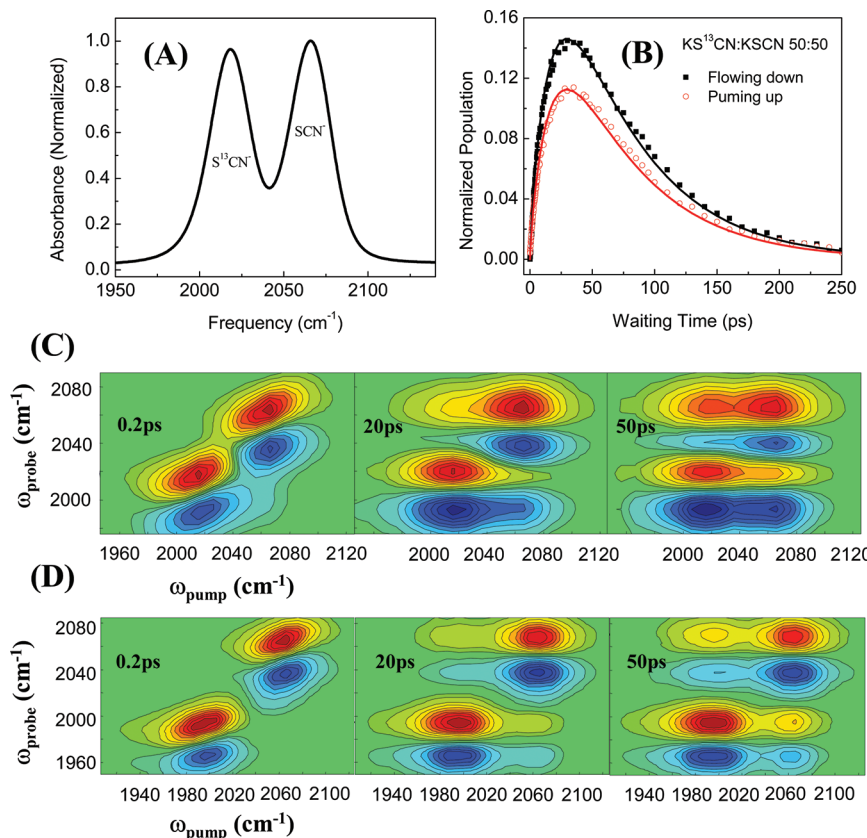


**Figure 1.** (A) FTIR spectra of 1:1  $\text{KS}^{13}\text{CN}$ /KSCN aqueous solution (10M). (B) Time-dependent intensities of energy transfer peaks between  $\text{S}^{13}\text{CN}^-$  and  $\text{SCN}^-$ . Square solid dots are from the flowing-down peaks ( $\text{SCN}^-$  to  $\text{S}^{13}\text{CN}^-$ ), and the circle open dots are from the pumping-up peaks ( $\text{S}^{13}\text{CN}^-$  to  $\text{SCN}^-$ ). Lines are calculations from the kinetic model. 2D IR spectra of (C)  $\text{KS}^{13}\text{CN}$ /KSCN and (D)  $\text{KS}^{13}\text{C}^{15}\text{N}$ /KSCN 10 M aqueous solutions at different waiting times.

Here, we used isotope-labeled KSCN aqueous solutions as model systems to examine the donor/acceptor energy mismatch and vibrational coupling strength dependences of the vibrational energy transfer rates between the nitrile stretches of the anions ( $\text{SCN}^-$ ,  $\text{S}^{13}\text{CN}^-$ , and  $\text{S}^{13}\text{C}^{15}\text{N}^-$ ). In the energy mismatch dependent experiments, we used different isotopes to label the anion to change the vibrational frequency of the nitrile stretch. Because the isotope labeling does not change the ionic interaction strength, the vibrational coupling strength among the anions remains essentially the same as that of the unlabeled anions. By this method, we were able to tune the energy mismatch between the donor and acceptor (the nitrile stretch of the isotope labeled or unlabeled  $\text{SCN}^-$  anions) without changing the coupling strength between the interacting nitrile groups or its fluctuation time. In the coupling strength dependent measurements, by changing the donor/acceptor population ratio, we were able to change the overall vibrational coupling strength between one donor and its acceptors without changing the energy mismatch. Experimental details and results are described in the following texts.

## 2. EXPERIMENTAL SECTION

The experimental setup has been described elsewhere.<sup>14,15,17</sup> Briefly, a ps amplifier and a fs amplifier are synchronized with the same seed pulse from a Ti-sapphire oscillator. The ps amplifier pumps an OPA to produce 0.7–1 ps Mid-IR pulses with a bandwidth  $\sim 21 \text{ cm}^{-1}$  ( $10\text{--}27 \text{ cm}^{-1}$ ) in a tunable frequency range from 500 to  $4000 \text{ cm}^{-1}$  with energy 1–40  $\mu\text{J}/\text{pulse}$  at 1 kHz. The fs

amplifier pumps another OPA to produce  $\sim 140 \text{ fs}$  Mid-IR pulses with a bandwidth  $\sim 200 \text{ cm}^{-1}$  in a tunable frequency range from  $500 \text{ cm}^{-1}$  to  $4000 \text{ cm}^{-1}$  with energy 1–40  $\mu\text{J}/\text{pulse}$  at 1 kHz. In 2D IR and pump/probe experiments, the ps IR pulse is the pump beam (pump power is adjusted based on need). The fs IR pulse is the probe beam which is frequency resolved by a spectrograph yielding the probe axis of a 2D IR spectrum. Scanning the pump frequency yields the other axis of the spectrum. Two polarizers are added into the probe beam path to selectively measure the parallel or perpendicular polarized signal relative to the pump beam. Vibrational lifetimes are obtained from the rotation-free 1–2 transition signal  $P_{\text{life}} = P_{\parallel} + 2 \times P_{\perp}$ , where  $P_{\parallel}$  and  $P_{\perp}$  are parallel and perpendicular data, respectively. Rotational relaxation times are acquired from  $\tau = (P_{\parallel} - P_{\perp}) / (P_{\parallel} + 2 \times P_{\perp})$ .

$\text{KS}^{13}\text{C}^{15}\text{N}$  and  $\text{KS}^{13}\text{CN}$  were purchased from Cambridge isotope laboratory and used without further purification.  $\text{D}_2\text{O}$  was from C/D/N Isotopes Inc. The liquid sample for the FTIR and 2D IR measurements were contained in a sample cell composed of two  $\text{CaF}_2$  windows separated by a Teflon spacer. The thickness of the spacer was adjusted based on the optical densities. The experimental optical path and apparatus were purged with clean air free of  $\text{CO}_2$  or water. All the measurements were carried out at room temperature (297 K).

## 3. RESULTS AND DISCUSSIONS

### 3.1. Energy Mismatch Dependence. 3.1.1. Nonresonant Energy Transfers between $\text{SCN}^-$ and $\text{S}^{13}\text{CN}^-$ and $\text{SCN}^-$ and $\text{S}^{13}\text{C}^{15}\text{N}^-$ .

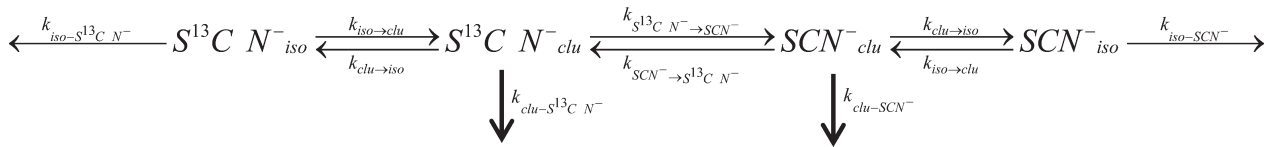


Figure 2. Illustration of the kinetic model.

KS<sup>13</sup>CN/KSCN aqueous solutions with a salt/water molar ratio 1/2.4 (10 M). The S<sup>13</sup>CN<sup>-</sup> isotope labeling shifts the CN stretch frequency from 2064 cm<sup>-1</sup> down to 2015 cm<sup>-1</sup>, allowing the nonresonant energy transfers between SCN<sup>-</sup> and S<sup>13</sup>CN<sup>-</sup> to be directly probed with 2D IR measurements.

We first use Figure 1C to interpret 2D IR spectra. Figure 1C displays three waiting time ( $T_w$ ) dependent 2D IR spectra of 1:1 KS<sup>13</sup>CN/KSCN solution at room temperature. The 0.2 ps panel corresponds to a very short  $T_w$ , at which negligible vibrational energy exchange has occurred. The red peaks (the 0–1 CN or <sup>13</sup>CN stretch transition) and blue peaks (1–2 transition) appear only on the diagonal. The blue peaks shift to lower frequencies along the  $y$ -axis because of vibrational anharmonicities. After a long waiting period ( $T_w = 50$  ps), additional peak pairs appear on the off-diagonal positions. These peaks arise from the vibrational energy exchange between S<sup>13</sup>CN<sup>-</sup> and SCN<sup>-</sup>. Each diagonal peak pair and its corresponding cross peak pair along the  $y$ -axis form an energy donor (diagonal)/acceptor (cross) pair. The relative cross/diagonal peak ratio indicates how fast the vibrational energy transfers from the donor to the acceptor. Comparing Figure 1C and D, we can see that the cross peaks of SCN<sup>-</sup>/S<sup>13</sup>C<sup>15</sup>N<sup>-</sup> (energy mismatch  $\sim 73$  cm<sup>-1</sup>) in (D) are obviously smaller than those of the SCN<sup>-</sup>/S<sup>13</sup>CN<sup>-</sup> with a smaller mismatch  $\sim 49$  cm<sup>-1</sup> in (C) at the same waiting time. This simple inspection qualitatively reveals that a system with a bigger energy mismatch has a smaller energy transfer rate. The following quantitative analysis confirms this conclusion.

To quantitatively analyze the energy transfer rates between S<sup>13</sup>CN<sup>-</sup> and SCN<sup>-</sup>, we used a slightly modified kinetic model from our previous work:<sup>3</sup> in the solution, some S<sup>13</sup>CN<sup>-</sup> and SCN<sup>-</sup> form clustered anions (denoted as S<sup>13</sup>CN<sup>-</sup><sub>clu</sub> and SCN<sup>-</sup><sub>clu</sub>), and the rest anions are separated (denoted as S<sup>13</sup>CN<sup>-</sup><sub>iso</sub> and SCN<sup>-</sup><sub>iso</sub>). These two types of anions (not frequency resolvable) are under dynamic equilibrium: they can exchange locations with rate constants  $k_{\text{clu} \rightarrow \text{iso}}$  and  $k_{\text{iso} \rightarrow \text{clu}}$  whose ratio is determined by the equilibrium constant  $K = (k_{\text{iso} \rightarrow \text{clu}})/(k_{\text{clu} \rightarrow \text{iso}})$ . The S<sup>13</sup>CN<sup>-</sup><sub>clu</sub> and SCN<sup>-</sup><sub>clu</sub> anions can exchange vibration energy with rate constants  $k_{\text{S}^{13}\text{CN}^- \rightarrow \text{SCN}^-}$  and  $k_{\text{SCN}^- \rightarrow \text{S}^{13}\text{CN}^-}$  whose ratio is determined by the detailed balance. Any separated anion cannot transfer vibrational energy to other anions. The vibrational excitation of each species decays with its own vibrational relaxation rate constant. Here, we want to emphasize one point: the assumption of ion clustering is the natural result of the inhomogeneous distribution of solute in a room temperature solution. At room temperature, because of the thermal fluctuation, some ions are always closer to each other while others are well separated in a liquid solution. These closer ions can be considered as clustered in the model. Therefore, it is not necessary that this model can only be applied to or depends on ion clustering. In the model, the vibrational lifetimes were determined with pump/probe experiments. The lifetimes of the isolated species were measured in very dilute solutions, and the lifetimes of the clustered species were measured in the saturated solutions. Because the environment of the energy transfers can be different from those where the lifetimes were measured, in the kinetic calculations we

allowed the vibrational lifetimes to vary in the range of 20% to best fit the data. The time dependent vibrational excitation populations were measured with 2D IR. In experiments, all data are rotation-free. Therefore, the model does not contain any rotational component. The model can be illustrated in Figure 2.

The model gives a series of differential equations. By numerically solving these equations and comparing the calculations from the solution to the experimental results, we obtained the energy transfer rate constants, the equilibrium constant and the location exchange rate constants. More details of the model are provided in the Supporting Information. The quantitative kinetic analysis of the 1:1 KSCN/KS<sup>13</sup>CN solution based on this location-energy-exchange model describes the experimental data very well (Figure 1B). It gives the energy transfer rate constant from SCN<sup>-</sup> to S<sup>13</sup>CN<sup>-</sup> ( $1/k_{\text{SCN}^- \rightarrow \text{S}^{13}\text{CN}^-}$ ) = 46 ± 7 ps, and the S<sup>13</sup>CN<sup>-</sup> to SCN<sup>-</sup> up-pumping time constant ( $1/k_{\text{S}^{13}\text{CN}^- \rightarrow \text{SCN}^-}$ ) = 60 ± 8 ps. The down-flowing and up-pumping rate ratio is determined by the detailed balance principle ( $(k_{\text{S}^{13}\text{CN}^- \rightarrow \text{SCN}^-}/k_{\text{SCN}^- \rightarrow \text{S}^{13}\text{CN}^-}) = \exp(-49/205) = 0.79$ ) with the donor/acceptor energy mismatch 49 cm<sup>-1</sup> at the experimental temperature 297 K. The equilibrium constant  $K$  is 40 ± 4, which corresponds to 97% of anions forming clusters, and the clustered and isolated anions exchange time constant  $1/k_{\text{clu} \rightarrow \text{iso}} = 10 \pm 5$  ps. When the same procedure was used, for the 1:1 KS<sup>13</sup>C<sup>15</sup>N/KSCN solution (Figure 1D), quantitative analyses<sup>3</sup> show that the equilibrium constant  $K$  is 40 ± 4, which corresponds to 97% of anions forming clusters, and the clustered and isolated anions exchange time constant  $1/k_{\text{clu} \rightarrow \text{iso}} = 12 \pm 7$  ps. These two values are consistent with the KS<sup>13</sup>CN/KSCN system. The energy transfer time constant from SCN<sup>-</sup> to S<sup>13</sup>C<sup>15</sup>N<sup>-</sup> (down-flowing) is  $1/k_{\text{down}} = 115 \pm 10$  ps, and the S<sup>13</sup>C<sup>15</sup>N<sup>-</sup> to SCN<sup>-</sup> up-pumping time constant is  $1/k_{\text{up}} = 164 \pm 15$  ps. The energy mismatch of nitrile stretch between KS<sup>13</sup>C<sup>15</sup>N and KSCN is 73 cm<sup>-1</sup>, bigger than the 49 cm<sup>-1</sup> between KS<sup>13</sup>CN and KSCN. This 24 cm<sup>-1</sup> energy mismatch difference slows down the energy transfer for more than two times (115 vs 46 ps).

**3.1.2. Resonant Energy Transfers Among S<sup>13</sup>C<sup>15</sup>N<sup>-</sup> Anions.** It is well-known that intermolecular resonant electronic energy transfers can induce anisotropy decays of fluorescence signal or pump/probe signal, which has been extensively applied into biological studies.<sup>18,19</sup> Following a similar mechanism, intermolecular resonant vibrational energy transfers can also induce anisotropy decays of vibrational third order optical signals. The energy transfer rate and the rate of anisotropy decay it induces in a certain environment have a certain well-defined correlation.<sup>20</sup> By measuring the rate of anisotropy decay induced by energy transfer, the rate of energy transfer can be obtained. However, in general, the vibrational pump/probe signal anisotropy decay is determined by two factors: molecular reorientations and resonance energy transfers among vibrationally excited and unexcited probe molecules. Energy transfer rates can be determined from anisotropy measurements only if these two factors can be distinguished.

In experiments, the contributions from molecular reorientation and vibrational energy transfers can be clearly distinguished

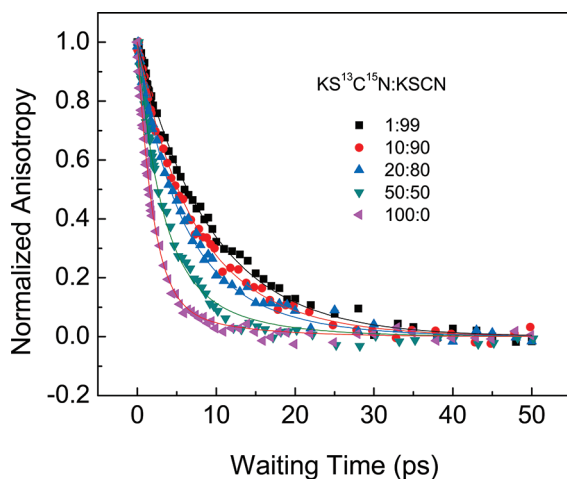


**Figure 3.** Anisotropy decay data (dots) of the <sup>13</sup>C<sup>15</sup>N stretch pump/probe signal of S<sup>13</sup>C<sup>15</sup>N<sup>-</sup> in 10 M aqueous solutions with different KS<sup>13</sup>C<sup>15</sup>N/KSCN molar ratios. Dots are data. Lines are calculations from eq 2.

by changing the resonant energy transfer rate through adjusting the number of resonant energy acceptors. In measuring the resonant energy transfer rate among the S<sup>13</sup>C<sup>15</sup>N anions in the 10 M aqueous solutions, we used different amounts of SCN<sup>-</sup> to replace S<sup>13</sup>C<sup>15</sup>N<sup>-</sup> in the solutions (the overall salt concentration remains constant) to adjust the number of resonant energy acceptors for the donor S<sup>13</sup>C<sup>15</sup>N<sup>-</sup>. The resonance energy transfer time constant among S<sup>13</sup>C<sup>15</sup>N<sup>-</sup> can then be obtained from such energy-acceptor-number dependent energy-transfer-induced anisotropy decay measurements.<sup>3,21</sup> Figure 3 displays the anisotropy decay of the pump/probe signal of S<sup>13</sup>C<sup>15</sup>N<sup>-</sup> as a function of delay time in the 10 M aqueous solutions with pure KS<sup>13</sup>C<sup>15</sup>N and mixtures of KS<sup>13</sup>C<sup>15</sup>N/KSCN with different isotope ratios. The anisotropy decay of the S<sup>13</sup>C<sup>15</sup>N<sup>-</sup> signal obviously becomes faster with the increase of the KS<sup>13</sup>C<sup>15</sup>N molar fraction, from 10 ps with 1% KS<sup>13</sup>C<sup>15</sup>N to 2.4 ps with 100% KS<sup>13</sup>C<sup>15</sup>N. This observation suggests that in solutions with high KS<sup>13</sup>C<sup>15</sup>N molar fractions, the resonant energy transfers among the S<sup>13</sup>C<sup>15</sup>N<sup>-</sup> anions contribute significantly to the anisotropy decay of the S<sup>13</sup>C<sup>15</sup>N<sup>-</sup> signal, because if only molecular rotations contribute to the anisotropy decay, more molar fractions of KS<sup>13</sup>C<sup>15</sup>N will not change the anisotropy decay or at most slow it down a little bit because of the slightly heavier atoms of the isotopes <sup>13</sup>C and <sup>15</sup>N rather than speed it up (observed).

It is straightforward to obtain the resonant energy transfer time constant from Figure 3. In the solution with 1% KS<sup>13</sup>C<sup>15</sup>N, the anisotropy decay (10 ps) is mostly caused by the molecular rotation, because the resonant energy donors and acceptors (S<sup>13</sup>C<sup>15</sup>N<sup>-</sup> anions) are well separated by the dominant SCN<sup>-</sup> anions so that the resonant energy will be slower than 240 ps (99\*2.4 ps). In addition, the nonresonant energy transfers between S<sup>13</sup>C<sup>15</sup>N<sup>-</sup> and SCN<sup>-</sup> is very slow (slower than 100 ps as analyzed above). Therefore, the anisotropy decay time constant  $\tau_{\text{or}} = 10 \pm 1$  ps of the solution with 1% KS<sup>13</sup>C<sup>15</sup>N can be considered as the molecular rotational time constant of S<sup>13</sup>C<sup>15</sup>N<sup>-</sup> in all the 10 M solutions, ignoring the very small influence caused by the mass differences among the C and N isotopes. In the solution with 100% KS<sup>13</sup>C<sup>15</sup>N, the anisotropy decay is from both molecular rotations and resonant energy transfers. Because the

molecular rotation time constant is  $\tau_{\text{or}} = 10 \pm 1$  ps and the time constant of anisotropy decay induced by both molecular rotation and energy transfers is  $t = 2.4$  ps, the resonant energy transfer time constant  $\tau$  is therefore 3 ps obtained from the correlation:  $1/\tau = 1/t - 1/(\tau_{\text{or}})$ .

To more rigorously analyze the resonant energy transfer kinetics, we adopt a revised version suggested by Prof. Robert Curl of our previous model, which can count the signal from each individual cluster to analyze the anisotropy data.<sup>3</sup> As we elaborated before, the ions in the 10 M KSCN/KS<sup>13</sup>C<sup>15</sup>N solutions form big clusters.<sup>3</sup> In the clusters, the anions can exchange vibrational energy through resonant or nonresonant processes. In a resonant energy transfer, the energy can exchange between one donor and one acceptor with the same forward and backward rate. In experiments, the probability for one anion to be vibrationally excited by our laser is low. Only about 0.5–1% of the anions are excited. Therefore, the number of the resonant energy acceptors is bigger than that of the energy donors in ion clusters of the same isotope unless the cluster contains only one or two anions. Because the probability of reverse transfer is inversely proportional to the number of acceptors: more acceptors resulting in statistically less likely reverse transfers, the originally laser induced vibrational excitation can dissipate away much faster than transfer back from the acceptors in bigger clusters. Based on the physical picture, in the resonant energy transfer kinetic analysis model we assume only a limited amount of acceptors isotropically orientated around one donor. This assumption allows us to use the classic correlation (the derivation is in Supporting Information) between the anisotropy decay rate constant  $k_{\text{ani}}$  and the resonant energy transfer rate constant  $k_{\text{eng}}$ :  $(k_{\text{ani}})/(k_{\text{eng}}) = 0.96$ . For simplicity, we approximate it into 1. The vibration energy can exchange among the donor and acceptors. For each energy transfer step from the original (laser excited) donor to one acceptor, or from one acceptor to another acceptor, the signal totally loses its anisotropy. Whenever the energy transfers back to the original donor, the anisotropy is recovered. In other words, the anisotropy is directly proportional to the time dependent number of the originally (laser) excited donor molecules. Therefore, fewer acceptors for one donor (corresponding to a smaller cluster, or more precisely, a smaller energy transfer unit) will result in slower energy-transfer-induced anisotropy decay. The mathematical derivation (in Supporting Information) of the model yields the following equation:

$$\frac{R(t)}{R(0)} = \frac{1}{n_{\text{tot}} \times c \times e^{-t/\tau_{\text{or}}}} [n_{\text{tot}} (c \times e^{-t/\tau} + 1 - c)^{n_{\text{tot}} - 1} \\ \times e^{-t/\tau} - (c \times e^{-t/\tau} + 1 - c)^{n_{\text{tot}}} + 1] \quad (2)$$

where  $\tau_{\text{or}}$  is the rotational time constant of S<sup>13</sup>C<sup>15</sup>N<sup>-</sup>,  $c$  is the percentage of S<sup>13</sup>C<sup>15</sup>N<sup>-</sup> (the energy carrier) among the isotopes, while  $n_{\text{tot}}$  is the number of anions (both S<sup>13</sup>C<sup>15</sup>N<sup>-</sup> and SCN<sup>-</sup>) in an energy transfer unit (a big cluster can have more than one energy transfer units).  $\tau$  is the resonant one-donor-to-one-acceptor energy transfer time constant.

In our experiment,  $\tau_{\text{or}} = 10 \pm 1.0$  ps is experimentally determined from the anisotropy measurement of the 1% KS<sup>13</sup>C<sup>15</sup>N 10 M solution, and  $c$  is the known experimental condition parameter. Calculations based on eq 2 with two adjustable parameters ( $\tau$  and  $n_{\text{tot}}$ ) simultaneously fit the five experimental sets of experimental anisotropy decay data very well. The analysis in Figure 3 yields  $\tau = 54 \pm 8$  ps, and  $n_{\text{tot}} = 18 \pm 3$ . This gives the total resonant energy transfer time constant among

**Table 1. Experimental and Calculated Energy Mismatch Dependence<sup>a</sup>**

	$\text{SCN}^- \rightarrow \text{S}^{13}\text{C}^{15}\text{N}^-$	$\text{SCN}^- \rightarrow \text{S}^{13}\text{CN}^-$	$\text{S}^{13}\text{C}^{15}\text{N}^- \rightarrow \text{S}^{13}\text{C}^{15}\text{N}^-$
energy mismatch ( $\text{cm}^{-1}$ )	73.0	49.0	0.0
experimental $1/k$ (ps)	$115 \pm 10$	$46 \pm 7$	$3 \pm 0.3$
calculated $1/k$ (ps)	108	54	5.7

<sup>a</sup> The calculation is based on eq 1 with  $\tau_c = 2.1$  ps and  $\langle \beta \rangle = 13.6 \text{ cm}^{-1}$ . The nonresonant energy transfer time constants are for the down-flowing process.

the  $\text{S}^{13}\text{C}^{15}\text{N}^-$  anions in the 100%  $\text{KS}^{13}\text{C}^{15}\text{N}$  10 M solution to be 3 ps (54/18 ps).

**3.1.3. Comparison between Experimental and Predicted Energy Mismatch Dependence.** The experimentally determined energy mismatch values and resonant and nonresonant (down-flowing) energy transfer time constants are listed in Table 1. The predicted energy transfer time constants based on eq 1 with  $\langle \beta \rangle = 13.6 \text{ cm}^{-1}$  (experimentally determined, see Supporting Information) and  $\tau_c = 2.1$  ps are also listed.  $\tau_c = 2.1$  ps is a semiempirical parameter. As discussed in our previous publication,<sup>15</sup> experimentally we cannot precisely determine the coupling fluctuation time  $\tau_c$ . Instead, we used the spectral diffusion time to take the place of the coupling fluctuation time because the environmental change can also cause the coupling to change. Even though the choice of  $\tau_c = 2.0 \pm 0.1$  ps (the time for 95% completion of the dynamic line width) was from the best fitting rather than any rigorous mathematical derivation. However, the spectral diffusion time  $\tau_c = 2.0 \pm 0.1$  ps has its chemical origin. As reported before, the molecular interaction enthalpies of many molecules are  $\leq 0.6$  kcal/mol.<sup>22</sup> According to our previous work,<sup>23–25</sup> the enthalpy values suggest that the dissociation times of these intermolecular interactions are  $\leq 2$  ps. In the series of work about room temperature liquids, we use  $\tau_c = 2.0 \pm 0.1$  ps as an empirical constant rather than a variable.

For the two nonresonant cases, the predictions fit experimental results (Table 1) very well. However, the prediction (5.7 ps) for the resonant case is about 100% slower than what (3 ps) is experimentally observed. Because the derivation of eq 1 is from the Fermi golden rule (in Supporting Information), in principle it should be applicable for both resonant and nonresonant energy transfers. Where does this inconsistency for the resonant and nonresonant energy transfers come from? The reason is quite interesting, shown in Figure 4.

As we discussed in above paragraphs, in the nonresonant energy transfer experiments,  $\text{SCN}^-$  and its isotope labeled  $\text{S}^{13}\text{C}^{15}\text{N}^-$  (or  $\text{S}^{13}\text{CN}^-$ ) are mixed with equal amount. Because experimentally the chance of vibrational excitation is small (0.5–1%), in an energy transfer unit (even the biggest unit has <20 anions), at most one anion is excited. Therefore, half ( $n_{\text{tot}}/2$ ) of the anions in this energy transfer unit will be the nonresonant energy acceptors for this donor. In the resonant energy transfer experiment, all anions are the same species ( $\text{S}^{13}\text{C}^{15}\text{N}^-$ ). For any energy donor, all anions except this donor in the energy transfer unit are resonant energy acceptors. Therefore, the number of resonant energy acceptors for this donor is  $n_{\text{tot}} - 1$ . The resonant energy acceptor number is about two times of that in the nonresonant case. Because the coupling constant for both resonant and nonresonant calculations with eq 1 is exclusively from the nonresonant energy transfer experiments, the prediction for the resonant energy transfer is only

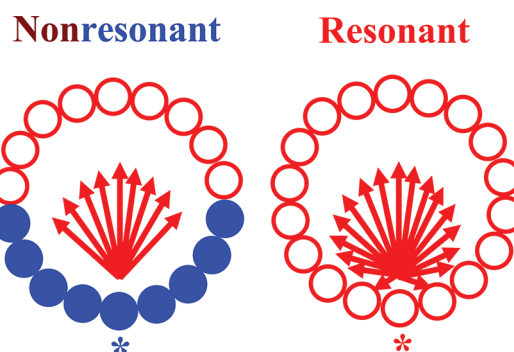


**Figure 4.** Pictorial explanation for the seemingly inconsistency of predictions from eq 1 for the nonresonant and resonant energy transfer experiments. In experiments, only one anion (the one with star) in an energy transfer unit can be excited. In the nonresonant case, 50% the anions are the nonresonant acceptors (the other isotope). However, in the resonant case, all anions except the donors are the resonant acceptor because all anions in the energy transfer unit are the same isotope. The acceptor number difference (~two times) counts for the inconsistency between the prediction and the resonant energy transfer experimental result.

for  $n_{\text{tot}}/2$  acceptors. The prediction for the resonant energy transfer must therefore be about 100% slower than what is measured due to this acceptor number difference. With the acceptor number normalized to the same number of energy acceptors in the calculation, based on the result of  $n_{\text{tot}} = 18$ , the experimental resonant energy time constant is  $5.7 \pm 0.6$  ps. This value is now consistent with the prediction from eq 1. The result can also be directly obtained from the resonant energy transfer measurement on the 50/50  $\text{KSCN}/\text{KS}^{13}\text{C}^{15}\text{N}$  mixture solution. The signal anisotropy of this sample in Figure 3 decays with a constant  $\sim 4$  ps, which gives the resonant energy transfer constant  $6.6 \pm 0.6$  ps, provided that the anion rotational time constant is 10 ps. Nonresonant energy transfer experiments with different donor/acceptor number ratios in the following further support this argument.

**3.2. Coupling Strength Dependence.** **3.2.1. Donor/Acceptor Number Ratio Dependence.** If the above explanation for the resonant energy transfer experiments is right, the up-pumping/down-flowing ratio of nonresonant energy transfers with donor/acceptor number ratios other than 1/1 will not be the Boltzmann factor  $e^{(-\hbar\omega_j)/(kT)}$  ( $\omega_{ij} = \omega_i - \omega_j$ ). Instead, the rate ratio will be the product of the Boltzmann factor times the donor/acceptor number ratio:

$$\frac{k_{ji}(\text{up-pumping})}{k_{ij}(\text{down-flowing})} = e^{-\omega_{ij}/RT} \times \frac{n_i}{n_j} \quad (\text{Eq.3})$$

eq Eq.3 is directly confirmed by the experimental results in Figure 5 of samples with different  $\text{KSCN}/\text{KS}^{13}\text{C}^{15}\text{N}$  ratios. In the  $\text{KSCN}/\text{KS}^{13}\text{C}^{15}\text{N}$  77/23 sample (Figure 5A), more energy acceptors (77) are available for the up-pumping process than the down-flowing process (23). Therefore, based on eq Eq.3, the up-pumping rate must be  $(77/23) \times e^{(-73/205)} = 2.3$  times of the down-flowing rate in this sample. From Figure 5A, energy up-pumping from  $\text{KS}^{13}\text{C}^{15}\text{N}$  to  $\text{KSCN}$  is obviously faster than the down-flowing process. Quantitative analysis based on the kinetic model in Figure 2 shows  $(k_{\text{up-pumping}})/(k_{\text{down-flowing}}) = 2.3$ , same as predicted by eq Eq.3. Data and calculations are shown in Figure 5A. For a similar reason, in the  $\text{KSCN}/\text{KS}^{13}\text{C}^{15}\text{N}$  25/75 sample (Figure 5C), the down-flowing rate will be much faster

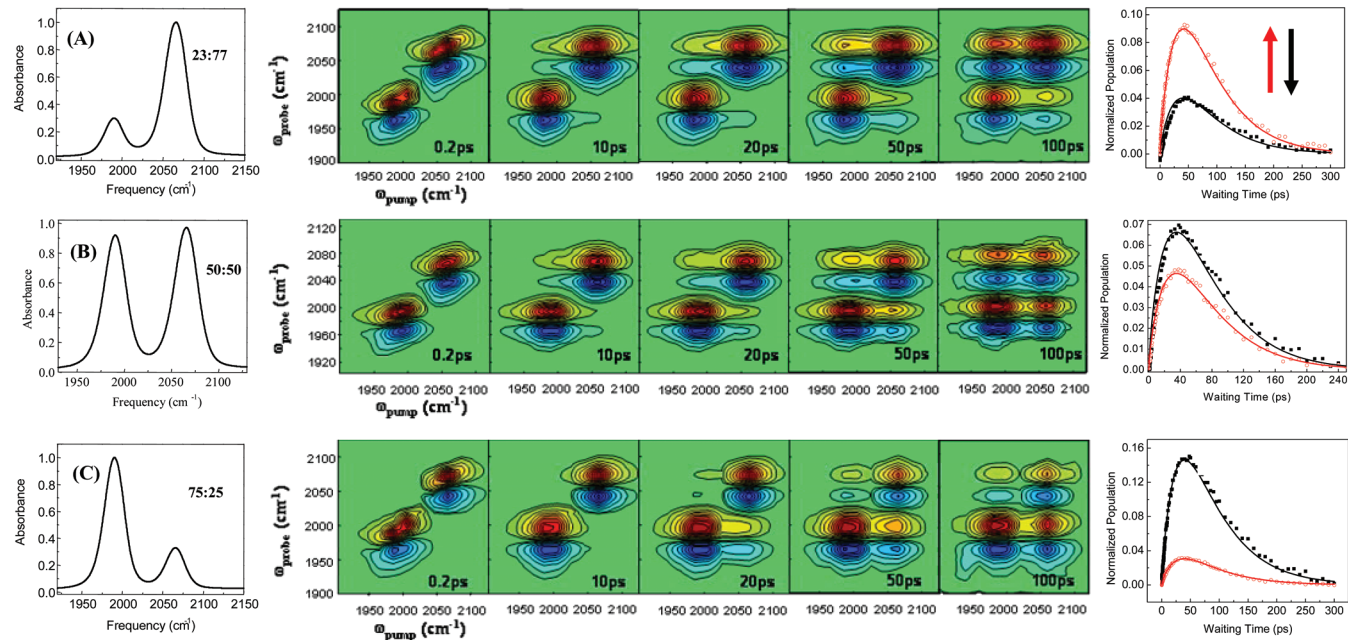


**Figure 5.** FTIR, 2D IR spectra, and waiting time dependent up-pumping and down-flowing cross peak intensities (points are data and curves are calculations based on the kinetic model) of 10 M aqueous solutions with different KSCN/KS<sup>13</sup>C<sup>15</sup>N ratios: (A) KSCN/KS<sup>13</sup>C<sup>15</sup>N = 77/23; (B) KSCN/KS<sup>13</sup>C<sup>15</sup>N = 50/50; (C) KSCN/KS<sup>13</sup>C<sup>15</sup>N = 25/75. At shortest waiting time, the intensities of two diagonal peak pairs in 2D IR spectra are normalized to be equal.

**Table 2. Calculated and Experimental Energy Transfer (Down-Flowing and Up-Pumping) Time Constants and Coupling Strengths for the Mixed KS<sup>13</sup>C<sup>15</sup>N/KSCN Aqueous Solution with Different Isotope Ratios<sup>a</sup>**

KS <sup>13</sup> C <sup>15</sup> N/KSCN	23:77	34:66	50:50	67:33	75:25
experimental $\langle \beta \rangle_{\text{down}}$ (cm⁻¹)	9.8 ± 4.0	11.9 ± 4.0	13.6 ± 3.0	16.2 ± 4.0	18.4 ± 5.0
experimental $\langle \beta \rangle_{\text{up}}$ (cm⁻¹)	17.3 ± 4.0	14.9 ± 3.0	13.6 ± 3.0	11.9 ± 4.0	9.8 ± 4.0
experimental $1/k_{\text{down}}$ (ps)	210 ± 30	143 ± 15	115 ± 10	68 ± 10	56 ± 8
experimental $1/k_{\text{up}}$ (ps)	94 ± 10	113 ± 15	164 ± 15	219 ± 20	267 ± 30
calcd $\langle \beta \rangle_{\text{down}}$ (cm⁻¹)	9.7 ± 0.7	11.8 ± 0.6	13.1 ± 0.6	17.1 ± 1.4	18.8 ± 1.4
calcd $\langle \beta \rangle_{\text{up}}$ (cm⁻¹)	17.4 ± 0.8	15.9 ± 0.9	13.2 ± 0.5	11.4 ± 0.5	10.4 ± 0.5
calcd $1/k_{\text{down}}$ (ps)	208 ± 80	141 ± 80	108 ± 50	76 ± 40	59 ± 30
calcd $1/k_{\text{up}}$ (ps)	95 ± 60	128 ± 70	154 ± 50	201 ± 90	296 ± 140

<sup>a</sup> The calculations are based on eq 1.

than the up-pumping rate. The rate ratio is 4.3. Only in the KSCN/KS<sup>13</sup>C<sup>15</sup>N 50/50 sample (Figure 5B), the rate ratio is determined by the Boltzmann factor  $k_{\text{up-pumping}}/k_{\text{down-flowing}} = 0.7$ . All the experimental energy transfer time constants are listed in Table 2.

**3.2.2. Coupling Strength Dependence.** The nonresonant energy transfer experiments with different donor/acceptor number ratios also provide an opportunity for us to examine the coupling strength dependent energy transfer rates without changing the donor/acceptor energy mismatch. In a sample where the donor/acceptor ratio is not 1/1, the effective coupling strength for the down-flowing process is different from that for the up-pumping process because the energy acceptor numbers for these two processes are different. Provided that the acceptors are identical, the total coupling strength  $\langle \beta_{1 \rightarrow n} \rangle$  from one donor to  $n$  acceptors is  $\sqrt{n} \times \langle \beta_{1 \rightarrow 1} \rangle$  from one donor to one acceptor:

$$\langle \beta_{1 \rightarrow n} \rangle = \sqrt{n} \langle \beta_{1 \rightarrow 1} \rangle \quad (\text{Eq.4})$$

It is well-known (as also been confirmed in the above) that

$$k_{i \rightarrow nj} = n \times k_{i \rightarrow j} \quad (\text{Eq.5})$$

It is then straightforward from eqs Eq.4 and Eq.5 to obtain  $k_{if} \propto \langle \beta_{if} \rangle^2$ , as stated in eq 1.

These correlations are consistent with experimental data. For example, in the KSCN/KS<sup>13</sup>C<sup>15</sup>N 77/23 sample (Figure 5A), the coupling strength  $\langle \beta_{\text{up-pumping}} \rangle$  of the up-pumping from S<sup>13</sup>C<sup>15</sup>N<sup>-</sup> to SCN<sup>-</sup> is for one donor to 77%  $n_{\text{tot}}$  acceptors, while the down-flowing coupling strength  $\langle \beta_{\text{down-flowing}} \rangle$  is for one donor to 23%  $n_{\text{tot}}$  acceptors. According to eq Eq.4,  $\langle \beta_{\text{up-pumping}} \rangle / \langle \beta_{\text{down-flowing}} \rangle = (77/23)^{1/2} = 1.8$ . Experimentally,  $\langle \beta_{\text{up-pumping}} \rangle / \langle \beta_{\text{down-flowing}} \rangle = 1.7$ . Within experimental uncertainty, the result fits the prediction very well. Based on this coupling ratio and eq 1,  $k_{\text{up-pumping}}/k_{\text{down-flowing}} = e^{-73/205} \times 1.8^2 = 2.3$ . Experimental results give  $k_{\text{up-pumping}}/k_{\text{down-flowing}} = (1/94)/(1/210) = 2.3$ . Again, experiments and predictions fit well. For other samples with different donor/acceptor population ratios, similar results

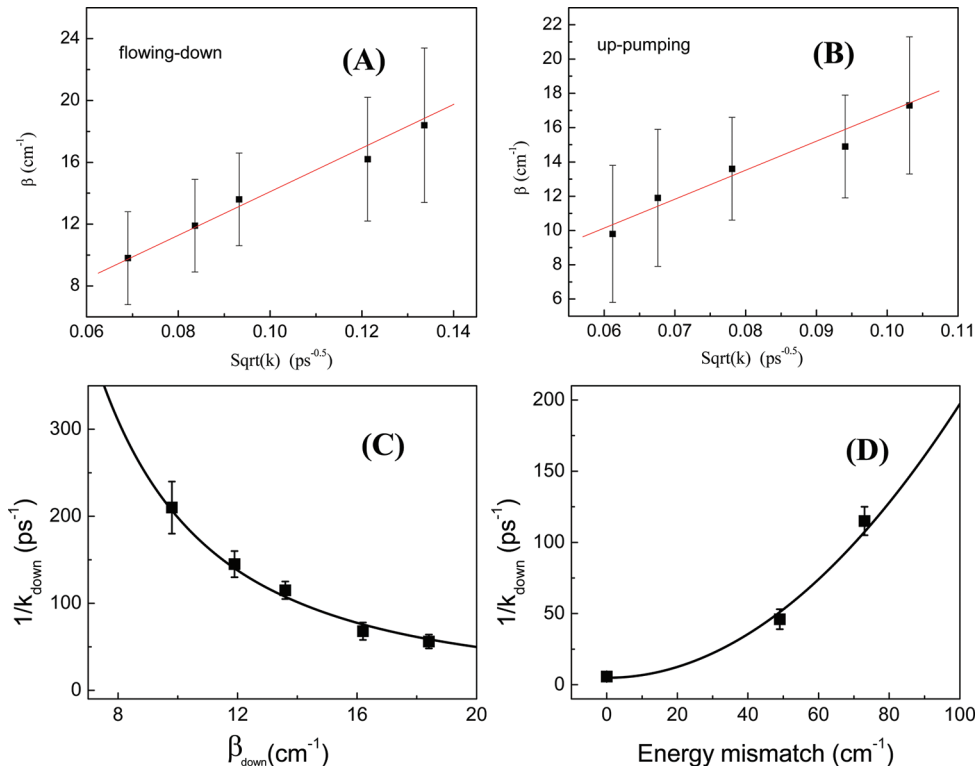


**Figure 6.** (A) Correlation between  $\langle\beta\rangle$  and  $k_{\text{flowing-down}}^{1/2}$ ; (B) Correlation between  $\langle\beta\rangle$  and  $k_{\text{up-pumping}}^{1/2}$ ; (C) The coupling strength dependence of the down-flowing energy transfer time constants of the  $\text{KS}^{13}\text{C}^{15}\text{N}/\text{KSCN}$  10 M solutions with a constant energy mismatch  $73 \text{ cm}^{-1}$ . (D) The energy mismatch dependence of the down-flowing energy transfer time constants with a constant average coupling strength  $13.6 \text{ cm}^{-1}$ . Dots are data and lines are calculations using eq 1 with  $\tau_c = 2.1 \text{ ps}$ .

are observed. Experimental and predicted coupling strength and energy transfer time constants are listed in Table 2. The experimental coupling strength and energy mismatch dependences and calculations based on eq 1 are plotted in Figure 6.

As shown in Figure 6, calculations based on eq 1 are consistent with experimental results. However, the uncertainty of the experimentally measured individual coupling strength is relatively big, resulting in a very big uncertainty in the calculated energy transfer rate constants. The big experimental uncertainty mainly comes from two factors: (1) the anharmonicities of vibrational coupling peaks are only a few wavenumbers, while the resolution of the spectrometer is  $1-2 \text{ cm}^{-1}$ ; (2) the bandwidth of the coupling red and blue peaks is  $\sim 30 \text{ cm}^{-1}$ , while their frequency difference is only a few wavenumbers, resulting in a severe spectral overlap. Experimentally, the energy transfer rates can be much more precisely determined. Therefore, in principle, eq 1 provides a better way for obtaining vibrational coupling strength with known energy transfer rates than the direct measurement with 2D IR methods. In this series of experiments, the determination of individual coupling strength through the 2D IR method has a relatively big uncertainty. However, the relative difference among the coupling strengths of samples with different donor/acceptor population ratios has a very small uncertainty. Therefore, the big uncertainty of the individual determination can possibly significantly affect the slopes of the straight lines in Figure 6A,B. Its effect on the linearity of the lines is relatively slight.

**3.3. Anion Distance Estimated with the Dipole–Dipole Approximation.** Under the dipole–dipole approximation,<sup>13,21,26</sup> the distance between an energy donor and its acceptor average

over all angles can be estimated with the following equation

$$\langle\beta\rangle = \frac{1}{4\pi\epsilon_0} \sqrt{\frac{2|\mu_D||\mu_A|}{3}} \frac{1}{r^3} \frac{1}{n^2} \quad (\text{Eq.6})$$

where  $r$  is the distance between the transition dipole moments of the donor and acceptor,  $\epsilon_0$  is the vacuum permittivity,  $\mu_i$  is the transition dipole moment of donor or acceptor,  $n$  is the refractive index of the solution,  $\langle\beta\rangle$  is the one-donor-to-one-acceptor coupling strength. In the 1:1  $\text{KS}^{13}\text{C}^{15}\text{N}/\text{KSCN}$  solution (10 M), the transition dipole moments of the nitrile stretches of  $\text{SCN}^-$  and  $\text{S}^{13}\text{C}^{15}\text{N}^-$   $\mu$  are determined to be  $0.39 \pm 0.03 \text{ D}$  based on FTIR measurements.<sup>20,27</sup> The averaged coupling strength is determined to be  $\langle\beta_{1-9}\rangle = 13.6 \text{ cm}^{-1}$  for one donor to nine acceptors. In eq Eq.6, the coupling strength  $\langle\beta\rangle$  is for one donor to one acceptor, which is  $\langle\beta\rangle = \langle\beta_{1-9}\rangle / 9^{1/2} = 4.5 \text{ cm}^{-1}$ . In the 10 M KSCN aqueous solution, the ion clusters are big and the environment for the energy transfer within the clusters is more like the melt KSCN salt rather than the salt/water mixture. Therefore, as suggested by literature,<sup>27</sup> the refractive index for eq Eq.6 is chosen to be 1.53 (the refractive index of the solid KSCN<sup>28</sup>) rather than the linear average value 1.46 based on the salt molar ratio in the solution we used before.<sup>3</sup>  $n = 1.53$  can also be derived from an empirical equation about the refractive index of KSCN aqueous solution.<sup>29</sup> With these improved parameters than those previously used,<sup>3</sup> the average distance between the transition dipole moments of the nitrile stretches of anions in the 1:1  $\text{KS}^{13}\text{C}^{15}\text{N}/\text{KSCN}$  10 M solution is determined to be  $4.0 \pm 0.3 \text{ \AA}$  based on eq Eq.6, slightly bigger than  $3.7 \pm 0.3 \text{ \AA}$  determined before.

The shortest C≡N distance in the KSCN crystal is also  $\sim 4.0 \text{ \AA}$ .<sup>30</sup> The similarity between the average anion distance in the clusters and that in the crystal is interesting. Even more interestingly, the nonresonant energy transfer rates between SCN<sup>-</sup> and S<sup>13</sup>C<sup>15</sup>N<sup>-</sup> in the KSCN/KS<sup>13</sup>C<sup>15</sup>N<sup>-</sup> 50/50 mixture crystal are the same as those in the 10 M aqueous solutions (data are in Supporting Information). Measurements on the KSCN/KS<sup>13</sup>C<sup>15</sup>N<sup>-</sup> crystalline samples also resolve a problem that we could not understand before. As analyzed in the resonant energy transfer part, the anions in 10 M aqueous solutions form clusters with more than 18 anions. According to the Einstein-Stokes equation,<sup>31</sup> the rotation of the clustered anions should be much slower (>18 times) than that of the free anions if the clusters are rigid. However, experimentally, the rotational relaxation time constant (10 ps) of anions in the clusters is only about three times slower than that (3.7 ps) of the free anions in water. Experiments on the KSCN crystalline samples give a very surprising plausible reason for this seemingly too fast rotational time (10 ps) of the clustered anions: the anions rotate in the KSCN crystal with a time constant 10 ps! Certainly, the rotation in crystal is hindered, different from that in the aqueous solutions where the anions can rotate to any angle. The anions in crystal can only wobble about 30° around the equilibrium positions. Data are in the Supporting Information. These observations, in addition to the fact that the number of anions in an energy transfer unit of the clusters is equal to the number of anions in the first solvation shell of any anion in the crystal,<sup>3</sup> seems to imply that the ion cluster structures in aqueous solutions share some similarities with their pure solid structure. However, we consider these similarities as qualitative rather than quantitative, because, as mentioned in the Introduction, (1) interactions other than the dipole–dipole interaction can also play roles, which may have different coupling strength/distance correlations from eq Eq.6, and (2) the experimentally determined distance is the transition dipole moment distance, which may or may not be the same as the bond distance. Nonetheless, future investigations on the KSCN and its isotope-labeled crystals provide an opportunity to quantitatively evaluate these factors, because the structures and the ionic distances of the crystals can be precisely determined with XRD.

#### 4. CONCLUDING REMARKS

In this work, we demonstrate that, in 10 M KSCN/KS<sup>13</sup>C<sup>15</sup>N or KSCN/KS<sup>13</sup>CN aqueous solutions, most of the anions form clusters. The cluster structure shares many similarities with that of the KSCN crystal. In the clusters, the nitrile groups of the anions can exchange their stretching vibrational energy through both resonant and nonresonant processes. Coupling strength and energy mismatch dependent experiments show that the kinetics of vibrational energy exchange among the clustered anions can be quantitatively described with an analytical equation derived from the Fermi golden rule. This equation mathematically connects energy transfer kinetics with the average vibrational coupling strength and other structural parameters, and therefore provides an important way to determine the coupling strength between two coupled oscillators through measuring the vibrational energy transfer kinetics. With the dipole–dipole approximation or other more precise descriptions (yet to be developed) about the vibrational coupling, the energy transfer rates can then be translated into interoscillator distances. This will hold promise for the vibrational energy transfer method to become an angstrom molecular ruler.

#### ■ ASSOCIATED CONTENT

**S Supporting Information.** Mathematical derivations and data on crystalline KSCN samples and liquid samples. This material is available free of charge via the Internet at <http://pubs.acs.org>.

#### ■ AUTHOR INFORMATION

##### Corresponding Author

\*E-mail: junrong@rice.edu.

#### ■ ACKNOWLEDGMENT

This material is based on work supported by the Welch foundation under Award No. C-1752 and the Air Force Office of Scientific Research under AFOSR Award No. FA9550-11-1-0070.

#### ■ REFERENCES

- (1) Bakker, H. J. *Chem. Rev.* **2008**, *108*, 1456.
- (2) Moilanen, D. E.; Wong, D.; Rosenfeld, D. E.; Fenn, E. E.; Fayer, M. D. *Proc. Natl. Acad. Sci. U.S.A.* **2009**, *106*, 375.
- (3) Bian, H. T.; Wen, X. W.; Li, J. B.; Chen, H. L.; Han, S. Z.; Sun, X. Q.; Song, J. A.; Zhuang, W.; Zheng, J. R. *Proc. Natl. Acad. Sci. U.S.A.* **2011**, *108*, 4737.
- (4) Deak, J. C.; Pang, Y.; Sechler, T. D.; Wang, Z.; Dlott, D. D. *Science* **2004**, *306*, 473.
- (5) Eaves, J. D.; Loparo, J. J.; Fecko, C. J.; Roberts, S. T.; Tokmakoff, A.; Geissler, P. L. *Proc. Natl. Acad. Sci. U.S.A.* **2005**, *102*, 13019.
- (6) Laage, D.; Hynes, J. T. *Proc. Natl. Acad. Sci. U.S.A.* **2007**, *104*, 11167.
- (7) Laage, D.; Hynes, J. T. *Science* **2006**, *311*, 832.
- (8) Bagchi, B. *Chem. Rev.* **2005**, *105*, 3197.
- (9) Lin, Y. S.; Auer, B. M.; Skinner, J. L. *J. Chem. Phys.* **2009**, *131*, 13.
- (10) Ji, M. B.; Odelius, M.; Gaffney, K. J. *Science* **2010**, *328*, 1003.
- (11) Marcus, Y.; Hefter, G. *Chem. Rev.* **2006**, *106*, 4585.
- (12) Leitner, D. M.; Havenith, M.; Gruebele, M. *Int. Rev. Phys. Chem.* **2006**, *25*, 553.
- (13) Förster, T. *Ann. Phys. Leipzig* **1948**, *2*, 55.
- (14) Bian, H. T.; Li, J. B.; Wen, X. W.; Zheng, J. R. *J. Chem. Phys.* **2010**, *132*, 184505.
- (15) Bian, H. T.; Wen, X. W.; Li, J. B.; Zheng, J. R. *J. Chem. Phys.* **2010**, *133*, 034505.
- (16) Bian, H. T.; Zhao, W.; Zheng, J. R. *J. Chem. Phys.* **2009**, *131*, 124501.
- (17) Bian, H. T.; Li, J. B.; Wen, X. W.; Sun, Z. G.; Song, J. A.; Zhuang, W.; Zheng, J. R. *J. Phys. Chem. A* **2011**, *115*, 3357.
- (18) Giepmans, B. N. G.; Adams, S. R.; Ellisman, M. H.; Tsien, R. Y. *Science* **2006**, *312*, 217.
- (19) Miyawaki, A.; Llopis, J.; Heim, R.; McCaffery, J. M.; Adams, J. A.; Ikura, M.; Tsien, R. Y. *Nature* **1997**, *388*, 882.
- (20) Scholes, G. D. *Ann. Rev. Phys. Chem.* **2003**, *54*, 57.
- (21) Woutersen, S.; Bakker, H. J. *Nature* **1999**, *402*, 507.
- (22) Fuchs, R.; Peacock, L. A.; Stephenson, W. K. *Can. J. Chem.* **1982**, *60*, 1953.
- (23) Zheng, J. R.; Fayer, M. D. *J. Am. Chem. Soc.* **2007**, *129*, 4328.
- (24) Zheng, J.; Fayer, M. D. *J. Phys. Chem. B* **2008**, *112*, 10221.
- (25) Zheng, J. *Ultrafast Chemical Exchange Spectroscopy*; VDM Verlag: Germany, 2008.
- (26) Gaffney, K. J.; Piletic, I. R.; Fayer, M. D. *J. Chem. Phys.* **2003**, *118*, 2270.
- (27) Knox, R. S.; van Amerongen, H. *J. Phys. Chem. B* **2002**, *106*, 5289.
- (28) Savoie, R.; Tremblay, J. *J. Opt. Soc. Am.* **1967**, *57*, 329.
- (29) Boström, J. M.; Williams, D. R. M.; Ninham, B. W. *Biol. J.* **2003**, *85*, 9.
- (30) Yamada, Y.; Watanabe, T. *Bull. Chem. Soc. Jpn.* **1963**, *36*, 1032.
- (31) Lamb, H. *Hydrodynamics*; Cambridge University Press: London, 1994.

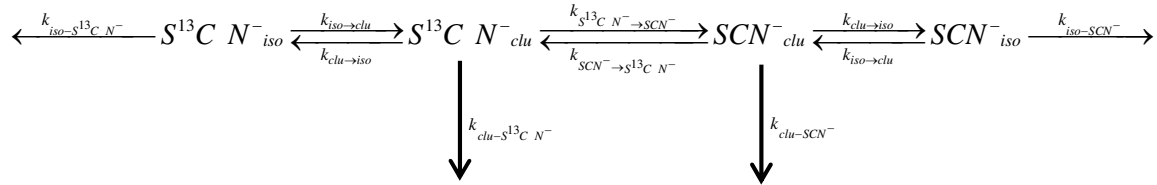
**Nonresonant and Resonant Mode-Specific Intermolecular  
Vibrational Energy Transfers in Electrolyte Aqueous Solutions**

**Hongtao Bian, Hailong Chen, Jiebo Li, Xiewen Wen, Junrong Zheng<sup>\*</sup>**

**Supporting material**

## The location-energy- exchange model

To quantitatively analyze the energy transfer kinetics between  $S^{13}CN^-$  and  $SCN^-$ , we created a location-energy-exchange kinetic model which can be described in the following scheme,



(Scheme.1)

Different from our previous model<sup>1</sup>, here the nitrile stretch vibrational lifetimes of separated ( $SCN^-_{iso}$  or  $S^{13}CN^-_{iso}$ ) and clustered anions ( $SCN^-_{clu}$  or  $S^{13}CN^-_{clu}$ ) are different. From the model, we derive four differential equations:

$$\frac{d[S^{13}CN^- *_{clu}(t)]}{dt} = -(k_{clu-S^{13}CN^-} + k_{clu \rightarrow iso} + k_{S^{13}CN^- \rightarrow SCN^-}) [S^{13}CN^- *_{clu}(t)] + k_{iso \rightarrow clu} [S^{13}CN^- *_{iso}(t)] + k_{SCN^- \rightarrow S^{13}CN^-} [SCN^- *_{clu}(t)] \quad \text{Eq. S(1)}$$

$$\frac{d[S^{13}CN^- *_{iso}(t)]}{dt} = -(k_{iso-S^{13}CN^-} + k_{iso \rightarrow clu}) [S^{13}CN^- *_{iso}(t)] + k_{clu \rightarrow iso} [S^{13}CN^- *_{clu}(t)] \quad \text{Eq. S(2)}$$

$$\frac{d[SCN^- *_{clu}(t)]}{dt} = -(k_{clu-SCN^-} + k_{clu \rightarrow iso} + k_{SCN^- \rightarrow S^{13}CN^-}) [SCN^- *_{clu}(t)] + k_{iso \rightarrow clu} [SCN^- *_{iso}(t)] + k_{S^{13}CN^- \rightarrow SCN^-} [S^{13}CN^- *_{clu}(t)] \quad \text{Eq. S(3)}$$

$$\frac{d[SCN^- *_{iso}(t)]}{dt} = -(k_{iso-SCN^-} + k_{iso \rightarrow clu}) [SCN^- *_{iso}(t)] + k_{clu \rightarrow iso} [SCN^- *_{clu}(t)], \quad \text{Eq. S(4)}$$

where \* represents vibrational excitation. The equations are numerically solved with initial conditions  $[S^{13}CN^- *_{clu}(0)] = \frac{K}{K+1}$ ,  $[S^{13}CN^- *_{iso}(0)] = \frac{1}{K+1}$ ,  $[SCN^- *_{clu}(0)] = [SCN^- *_{iso}(0)] = 0$  if  $S^{13}CN^-$  is initially excited.  $[S^{13}CN^- *_{clu}(t)] + [S^{13}CN^- *_{iso}(t)]$  and  $[SCN^- *_{clu}(t)] + [SCN^- *_{iso}(t)]$  are experimentally determined. Similar expressions are applied if  $SCN^-$  is initially excited.

Both CN vibrational decays are experimentally observed to be bi-exponential. Vibrational bi-exponential decay is frequently observed for modes in the range of 2000~2300 cm<sup>-1</sup><sup>2,5</sup>. It has been attributed to the fast vibrational equilibrium between the bright mode and one coupled dark mode<sup>2</sup>. Here, we adopted the method we developed for bi-exponential decays to analyze the kinetics<sup>2,4,5</sup>. We separate each CN stretch into two subgroups. The weighing factor of each subgroup is determined by the prefactors of the bi-exponential. Each subgroup has a single-exponential-decay lifetime time. Each

subgroup can exchange energy with other CN stretches, but the subgroups can't exchange energy with each other (this follows the assumed physical picture of bi-exponential: the sub-components can be considered as independent species). In the model, the effects of dynamics: spectral diffusions, vibrational decays and vibrational exchanges within each species are simply treated as apparent vibrational decays as experimentally measured.

The experimentally determined vibrational decay rate constants include the effect of energy transfer. Therefore, in calculations, they are allowed to vary by 10%. The other parameters, specifically the exchange rate constants and the equilibrium constant are not known beforehand. Because the ratio of the location exchange rate constants is the equilibrium constant and the ratio of the energy transfer rate constants is determined by

the detailed balance( $\frac{k_{S^{13}CN^- \rightarrow SCN^-}}{k_{SCN^- \rightarrow S^{13}CN^-}} = \exp(-\frac{49}{205}) = 0.79$ ), there are only three unknown

parameters in the calculations.

The experimental results and calculations with detailed input and out parameters for 1:1  $KS^{13}CN/KSCN$  and 1:1  $KS^{13}C^{15}N/KSCN$  solutions are displayed in fig. S1 and S2.

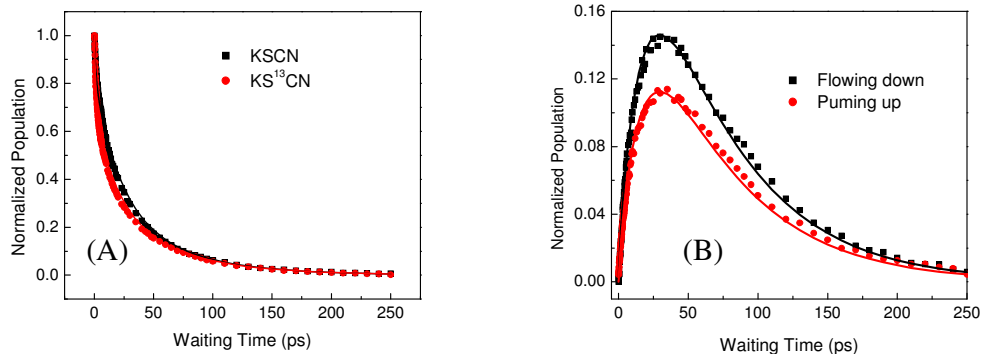


**Figure S1.** Data and calculations of nonresonance [(A): diagonal peak intensities and (B): cross peak intensities] for a 50%:50%  $KS^{13}CN/KSCN$  aqueous solution. Dots are data, and lines are calculations. Calculations for (A) and (B) are with input parameters:

$$\begin{aligned} k_{clu-SCN^- fast} &= 1/2.5 (ps^{-1}); k_{clu-SCN^- slow} &= 1/60.0 (ps^{-1}); k_{clu-S^{13}CN^- fast} &= 1/2.0 (ps^{-1}); k_{clu-S^{13}CN^- slow} &= 1/59.0 (ps^{-1}); \\ k_{iso-SCN^- fast} &= 1/1.5 (ps^{-1}); k_{iso-SCN^- slow} &= 1/20.0 (ps^{-1}); k_{iso-S^{13}CN^- fast} &= 1/1.6 (ps^{-1}); k_{iso-S^{13}CN^- slow} &= 1/24.0 (ps^{-1}); \\ k_{clu \rightarrow iso} &= 1/10.0 (ps^{-1}); K=40; k_{SCN^- \rightarrow S^{13}CN^-} &= 1/46 (ps^{-1}); D=0.78 \end{aligned}$$

with pre-factors of the subgroups and offset of the bi-exponential

$$A_{clu-SCN^- fast} = A_{iso-SCN^- fast} = 0.15; A_{clu-SCN^- slow} = A_{iso-SCN^- slow} = 0.85;$$

$$A_{clu-S^{13}CN^- fast} = A_{iso-S^{13}CN^- fast} = 0.30; A_{clu-S^{13}CN^- slow} = A_{iso-S^{13}CN^- slow} = 0.70; offset = 0$$

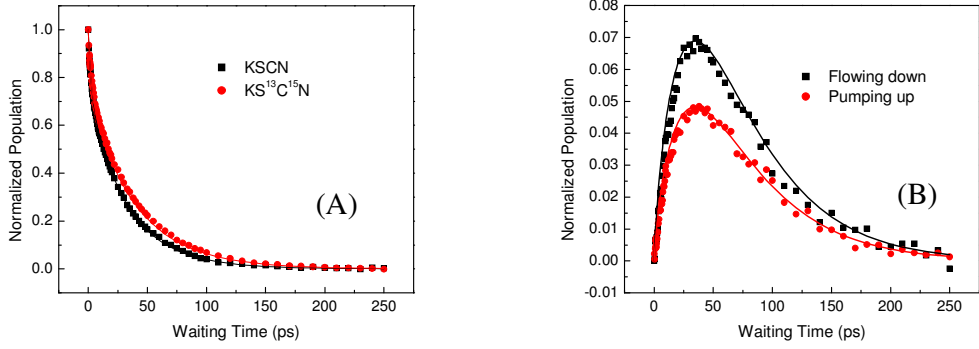


**Figure S2.** Data and calculations of nonresonance [(A) and (B)] for a 50%:50%  $KS^{13}C^{15}N/KSCN$  aqueous solution. Dots are data, and lines are calculations. Calculations for (A) and (B) are with input parameters:

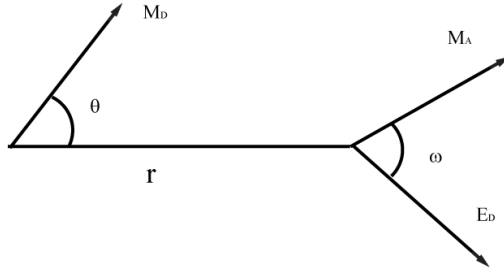
$$\begin{aligned}
 k_{clu-SCN^- fast} &= 1/2.5 (ps^{-1}); k_{clu-SCN^- slow} = 1/45.0 (ps^{-1}); k_{clu-S^{13}C^{15}N^- fast} = 1/2.3 (ps^{-1}); k_{clu-S^{13}C^{15}N^- slow} = 1/55.0 (ps^{-1}); \\
 k_{iso-SCN^- fast} &= 1/1.8 (ps^{-1}); k_{iso-SCN^- slow} = 1/20.0 (ps^{-1}); k_{iso-S^{13}C^{15}N^- fast} = 1/1.7 (ps^{-1}); k_{iso-S^{13}C^{15}N^- slow} = 1/28.0 (ps^{-1}); \\
 k_{clu \rightarrow iso} &= 1/12.0 (ps^{-1}); K=40; k_{SCN^- \rightarrow S^{13}C^{15}N^-} = 1/115 (ps^{-1}); D=0.7
 \end{aligned}$$

with pre-factors of the subgroups and offset of the bi-exponential

$$\begin{aligned}
 A_{clu-SCN^- fast} &= A_{iso-SCN^- fast} = 0.25; A_{clu-SCN^- slow} = A_{iso-SCN^- slow} = 0.75; \\
 A_{clu-S^{13}C^{15}N^- fast} &= A_{iso-S^{13}C^{15}N^- fast} = 0.25; A_{clu-S^{13}C^{15}N^- slow} = A_{iso-S^{13}C^{15}N^- slow} = 0.75; \text{ offset} = 0
 \end{aligned}$$

**Derivation of**  $\frac{k_{\text{anisotropy}}}{k_{\text{energy}}} = 0.96$

The derivation follows how FRET changes the anisotropy of a molecule.



In a vibrational resonance energy transfer process, the orientational factor for the donor-acceptor pair is

$$\kappa^2 = (3 \cos^2 \theta + 1) \cos^2 \omega$$

where  $\theta$  being the angle between the donor transition moment and the direction joining donor and acceptor and  $\omega$  being the angle between the electric field of the donor at the acceptor and the acceptor transition moment (as shown in the figure above).

For simplicity, the molecules are assumed to be immobile and the excited state is assumed to remain localized on the originally excited molecule. Then neglecting the effects of rotational diffusion and only considering the situation at t=0, the probability for transfer depends on  $\theta$  and  $\omega$  according to

$$W(\theta, \omega) \propto (3 \cos^2 \theta + 1) \cos^2 \omega$$

During the energy transfer, the donor transition moment is rotated by an angle  $\psi$ , so as to coincide with its own electric field at the acceptor. Then it is rotated from this new orientation by an angle  $\omega$  so that it coincides finally with the acceptor transition moment. If the angular jump of  $\psi$  or  $\omega$  is equally probable in all azimuths, the final anisotropy of acceptor emission for a given pair  $(\psi, \omega)$  is

$$r_A(\psi, \omega) = r_D \frac{1}{4} (3 \cos^2 \psi - 1) (3 \cos^2 \omega - 1)$$

or

$$r_A(\theta, \omega) = \frac{1}{10} \left( \frac{3(3 \cos^2 \theta - 1)^2}{3 \cos^2 \theta + 1} - 1 \right) (3 \cos^2 \omega - 1)$$

Here, we have made use of the result  $r_D = \frac{2}{5}$  and the fact that  $\cos\psi = \frac{3\cos^2\theta - 1}{\sqrt{3\cos^2\theta + 1}}$  which can be obtained from the form of the electric field of a static dipole.

Thus, the anisotropy of a molecule can be obtained

$$\begin{aligned}
 r_A &= \frac{\int_0^\pi \int_0^\pi W(\theta, \omega) r_A(\theta, \omega) \sin \theta d\theta \sin \omega d\omega}{\int_0^\pi \int_0^\pi W(\theta, \omega) \sin \theta d\theta \sin \omega d\omega} \\
 &= \frac{\int_0^\pi \int_0^\pi (3\cos^2\theta + 1) \cos^2\omega \cdot \frac{1}{10} \left( \frac{3(3\cos^2\theta - 1)^2}{3\cos^2\theta + 1} - 1 \right) (3\cos^2\omega - 1) \cdot \sin \theta d\theta \sin \omega d\omega}{\int_0^\pi \int_0^\pi (3\cos^2\theta + 1) \cos^2\omega \sin \theta d\theta \sin \omega d\omega} \\
 &= \frac{1}{10} \frac{4}{5} \cdot \frac{8}{2} \cdot \frac{15}{3} = 0.016 = 4\% \times 0.4
 \end{aligned}$$

Finally, it is shown that a single resonance energy transfer step can reduce the anisotropy to 4% of the initial value. In other words, the anisotropy decay rate constant is only 96% of the energy transfer rate constant.

## Derivation of Eq. (2)

During resonance energy transfers, the energy can be transferred back from acceptors to the original donor. The probability of back transfer is inversely proportional to the number of acceptors: more acceptors have fewer back transfers. In experiments, once the energy is transferred from the donor to any acceptor, the anisotropy will decay. However, when a back transfer occurs, the anisotropy is recovered. Therefore, fewer acceptors for one donor will result in slower energy-transfer-induced anisotropy decay. In the model, the anisotropy is directly proportional to the time dependent number of excited donor molecules. A new kinetic equation can therefore be derived as stated in the following.<sup>1</sup> The rate equation for the probability  $p_i(t)$  of that molecule  $i$  is excited at time  $t$  is

$$\frac{dp_i(t)}{dt} = \sum_{j \neq i} k_{ij} p_j(t) - \sum_{j \neq i} k_{ji} p_i(t). \quad \text{Eq. S(5)}$$

$k_{ij}$  is the transfer rate between molecules  $i$  and  $j$ . For resonance energy transfers,  $k_{ij} = k_{ji} = k$ . In Eq. S(5), we only consider the energy transfer processes which are involved in changing anisotropy. The vibrational decay is thus not considered here. Then we have

$$\frac{dp_i(t)}{dt} = k \sum_{j \neq i} p_j(t) - k \sum_{j \neq i} p_i(t) = k[1 - p_i(t)] - k(n-1)p_i(t) = k[1 - np_i(t)], \quad \text{Eq. S(6)}$$

where  $n$  is the number of the donor and acceptor molecules. Assuming molecule “1” (the donor) is excited in a cluster at time 0, with the initial conditions

$$p_1(0) = 1, \quad p_i(0) = 0 \quad (i \neq 1). \quad \text{Eq. S(7)}$$

Solving Eq. S(6), we obtain

$$p_1(t) = \left(1 - \frac{1}{n}\right)e^{-knt} + \frac{1}{n} = \left(1 - \frac{1}{n}\right)e^{-\frac{nt}{\tau}} + \frac{1}{n}, \quad p_i(t) = 1 - p_1(t) \quad (i \neq 1). \quad \text{Eq. S(8)}$$

where  $\tau$  is the resonant one-donor-to-one-acceptor energy transfer time constant. In anisotropy decay for a given ( $n, m$ ) cluster where let  $m$ =number of  $S^{13}C^{15}N^-$  in a cluster of  $n$  anions. Let the mole fraction of the normal species by  $X_2$  and of  $S^{13}C^{15}N^-$  be  $X_1$ . The anisotropy decay upon excitation of  $S^{13}C^{15}N^-$  is given by

$$[R(t)]_m = e^{-t/\tau_{or}} [(1 - m^{-1})e^{-mt/\tau} + m^{-1}] [R(0)]_m \quad \text{Eq. S(9)}$$

where  $\tau_{or}$  is the rotational time constant of clustered  $S^{13}C^{15}N^-$ . The probability that there will be a species excited in an ( $n, m$ ) cluster is proportional to  $m$ . Thus the signal from a given cluster is

$$[R(t)]_m = e^{-t/\tau_{or}} [(1 - m^{-1})e^{-mt/\tau} + m^{-1}] m [R(0)]_1 \quad \text{Eq. S(10)}$$

and the total signal summed over the clusters will be

$$R(t)_n = \sum_{m=1}^n \frac{n!}{m!(n-m)!} X_1^m X_2^{n-m} m e^{-t/\tau_{or}} [(1-m^{-1})e^{-mt/\tau} + m^{-1}] [R(0)]_1 \quad \text{Eq. S(11)}$$

This can be analyzed using the binomial moment generating function.

$$R(t)_n = [R(0)]_1 e^{-t/\tau_{or}} \sum_{m=1}^n \binom{n}{m} X_1^m X_2^{n-m} [(m-1)e^{-mt/\tau} + 1] = [R(0)]_1 e^{-t/\tau_{or}} \left[ \sum_{m=1}^n \binom{n}{m} X_1^m X_2^{n-m} (m e^{-mt/\tau} - e^{-mt/\tau} + 1) \right] \quad \text{Eq. S(12)}$$

The quantity inside the bracket equals zero when  $m=0$  because the first term vanishes and the second and third term cancel each other. Thus we can change the sum from starting with  $m=1$  to starting with  $m=0$ .

$$R(t)_n = [R(0)]_1 e^{-t/\tau_{or}} \left[ \sum_{m=0}^n \binom{n}{m} X_1^m X_2^{n-m} (m e^{-mt/\tau} - e^{-mt/\tau} + 1) \right] \quad \text{Eq. S(13)}$$

The last term after summing equals 1. The middle term after summing is the binomial moment generating function and the first term is the first derivative of the moment generating function with respect to  $t$ . Using the equations from Wolfram Research (<http://mathworld.wolfram.com/BinomialDistribution.html>) and realizing that the first term is the derivative of the second by the quantity  $-t/\tau$ , we have

$$R(t)_n = [R(0)]_1 e^{-t/\tau_{or}} \{ n[X_1 e^{-t/\tau} + X_2]^{n-1} X_1 e^{-t/\tau} - [X_1 e^{-t/\tau} + X_2]^n + 1 \} \quad \text{Eq. S(14)}$$

When  $t = 0$ , we have

$$R(0)_n = [R(0)]_1 \{ nX_1 - 1 + 1 \} = [R(0)]_1 nX_1 \quad \text{Eq. S(15)}$$

Thus

$$R(t)_n / R(0)_n = n^{-1} X_1^{-1} e^{-t/\tau_{or}} \{ n[X_1 e^{-t/\tau} + X_2]^{n-1} X_1 e^{-t/\tau} - [X_1 e^{-t/\tau} + X_2]^n + 1 \} \quad \text{Eq. S(16)}$$

We use  $c$  to denote  $X_1$   $n_{tot}$  to denote  $n$ , the above equation is then converted into following expression.

$$\frac{R(t)}{R(0)} = \frac{1}{\frac{-t}{\tau_{or}} [n_{tot} (c \times e^{-\frac{t}{\tau}} + 1 - c)^{n_{tot}-1} c \times e^{-\frac{t}{\tau}} - (c \times e^{-\frac{t}{\tau}} + 1 - c)^{n_{tot}} + 1]} \quad \text{Eq. S(17)}$$

## Derivation of Eq. (1)

The energy transfer rate from vibrational state  $i$  to state  $j$  can be described from the Fermi's golden rule as<sup>4,6</sup>

$$k_{ij} = \gamma_{ij} \int_{-\infty}^{\infty} dt \exp(i\omega_{ij}t) \left\langle \frac{1}{2} \delta\beta(t), \delta\beta(0) \right\rangle_+ \quad \text{Eq. S(18)}$$

where  $\gamma_{ij} = \frac{1}{1 + \exp(-\frac{\hbar\omega_{ij}}{kT})}$  counts for the detailed balance.  $\omega_{ij}$  is the energy difference.

$\delta\beta(t)$  is a time dependent vibrational coupling between the two states as modulated by the bath.  $\tau_c$  is the coupling correlation time. If we assume this correlation function to be a single exponential with a time constant  $\tau_c$ , and further assume that  $\tau_c$  is the spectral diffusion time, Eq. S(18) can be rewritten as

$$k_{ij} = \gamma_{ij} \langle \delta\beta^2 \rangle \frac{\tau_c^{-1}}{\tau_c^{-2} + \omega_{ij}^2} \quad \text{Eq. S(19)}$$

If we further assume that the fluctuation of vibrational coupling  $\delta\beta$  is equal to the average coupling strength  $\langle \beta \rangle$  and  $\langle \beta^2 \rangle = \langle \beta \rangle^2$ , Eq. S(19) becomes

$$k_{ij} = \gamma_{ij} \langle \beta \rangle^2 \frac{\tau_c^{-1}}{\tau_c^{-2} + \omega_{ij}^2} \quad \text{Eq. S(20)}$$

For the resonant energy transfer condition ( $\omega_{ij} = 0$ ), Eq. S(20) becomes  $k_{ij} = \frac{1}{2} \langle \beta \rangle^2 \frac{\tau_c^{-1}}{\tau_c^{-2}}$ , which can also be directly derived from the 1<sup>st</sup> order perturbation<sup>7</sup>:

$$\langle i | T(t,0) | f \rangle = -\frac{i}{\hbar} \int_{t_0}^t \langle i | V(t') | f \rangle e^{-i\omega_{if}t'} dt', \quad \text{Eq. S(21)}$$

where  $i$  and  $f$  are the initial and final states, respectively, w  $T(t,0)$  is the transition operator.  $V(t')$  is the time dependent coupling.  $\omega_{if}$  is the energy mismatch of the two states. In our system for the resonant case,  $i = f$ .  $V(t')$  is assumed to be a single exponential decay:

$$V(t') = V \times e^{-t'/\tau} \quad \text{Eq. S(22)}$$

From Eq. S(21) and S(22), the resonant energy transfer rate equation can be derived:

$$p = \left| \langle i | T(t,0) | f \rangle \right|^2 = \left| -\frac{i}{\hbar} \int_0^t \langle V \rangle e^{-t'/\tau} dt' \right|^2 = \frac{V^2}{\hbar^2} \frac{(1 - e^{-t/\tau})^2}{\tau^2} = \frac{V^2}{E_\tau^2} (1 - e^{-t/\tau})^2, \quad \text{Eq. S(23)}$$

where  $p$  is the probability of energy transfer, and  $E_\tau$  is the energy corresponding to the decay time constant  $\tau$ . The energy transfer rate constant is therefore

$$k = \frac{dp}{dt} = \left(\frac{V}{E_\tau}\right)^2 \frac{d(1-e^{-t/\tau})^2}{dt} \cong \left(\frac{V}{E_\tau}\right)^2 \frac{2}{\tau} \times ((1-e^{-t/\tau}) \times e^{-t/\tau})_{\max} = \left(\frac{V}{E_\tau}\right)^2 \frac{2}{\tau} \times \frac{1}{4}$$

$$= \frac{1}{2} \times \left(\frac{V}{E_\tau}\right)^2 \times \frac{1}{\tau}$$

Eq.S(24)

Eq. S(24) is identical to what is obtained from Eq.S(20) for the resonant case. So, Eq.S(20) should be in principle applicable to both resonant and nonresonance energy transfers.

Fitting parameters for the time dependent intensities of the diagonal peaks (A) and the cross peaks (B) of the mixed  $\text{KS}^{13}\text{C}^{15}\text{N}/\text{KSCN}$  aqueous solutions with different ratios.

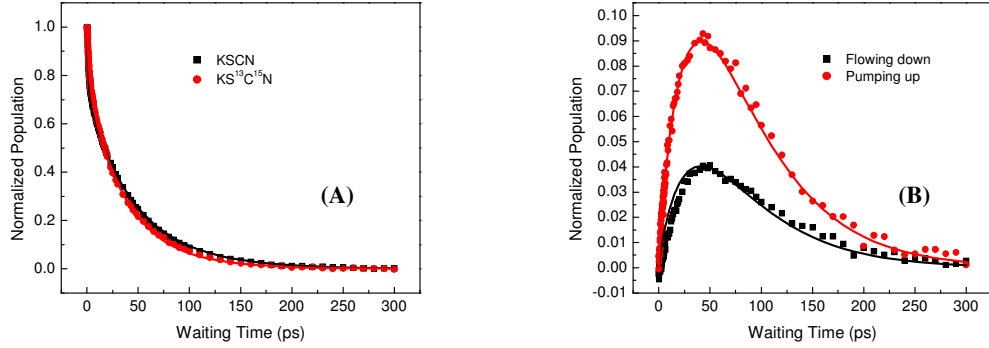


**Figure S3.** Data and calculations of nonresonance [(A) and (B)] for a 23%:77%  $\text{KS}^{13}\text{C}^{15}\text{N}/\text{KSCN}$  aqueous solution. Dots are data, and lines are calculations. Calculations for (A) and (B) are with input parameters:

$$\begin{aligned} k_{\text{clu}-\text{SCN}^{\sim}\text{fast}} &= 1/2.2 (\text{ps}^{-1}); k_{\text{clu}-\text{SCN}^{\sim}\text{slow}} = 1/58.0 (\text{ps}^{-1}); k_{\text{clu}-\text{S}^{13}\text{C}^{15}\text{N}^{\sim}\text{fast}} = 1/2.6 (\text{ps}^{-1}); k_{\text{clu}-\text{S}^{13}\text{C}^{15}\text{N}^{\sim}\text{slow}} = 1/62.0 (\text{ps}^{-1}); \\ k_{\text{iso}-\text{SCN}^{\sim}\text{fast}} &= 1/1.4 (\text{ps}^{-1}); k_{\text{iso}-\text{SCN}^{\sim}\text{slow}} = 1/21.0 (\text{ps}^{-1}); k_{\text{iso}-\text{S}^{13}\text{C}^{15}\text{N}^{\sim}\text{fast}} = 1/1.8 (\text{ps}^{-1}); k_{\text{iso}-\text{S}^{13}\text{C}^{15}\text{N}^{\sim}\text{slow}} = 1/28.0 (\text{ps}^{-1}); \\ k_{\text{clu} \rightarrow \text{iso}} &= 1/10.0 (\text{ps}^{-1}); K=40; k_{\text{SCN}^{\sim} \rightarrow \text{S}^{13}\text{C}^{15}\text{N}^{\sim}} = 1/210 (\text{ps}^{-1}); D=2.23 \end{aligned}$$

with pre-factors of the subgroups and offset of the bi-exponential

$$\begin{aligned} A_{\text{clu}-\text{SCN}^{\sim}\text{fast}} &= A_{\text{iso}-\text{SCN}^{\sim}\text{fast}} = 0.25; A_{\text{clu}-\text{SCN}^{\sim}\text{slow}} &= A_{\text{iso}-\text{SCN}^{\sim}\text{slow}} = 0.75; \\ A_{\text{clu}-\text{S}^{13}\text{C}^{15}\text{N}^{\sim}\text{fast}} &= A_{\text{iso}-\text{S}^{13}\text{C}^{15}\text{N}^{\sim}\text{fast}} = 0.25; A_{\text{clu}-\text{S}^{13}\text{C}^{15}\text{N}^{\sim}\text{slow}} &= A_{\text{iso}-\text{S}^{13}\text{C}^{15}\text{N}^{\sim}\text{slow}} = 0.75; \text{ offset} = 0 \end{aligned}$$

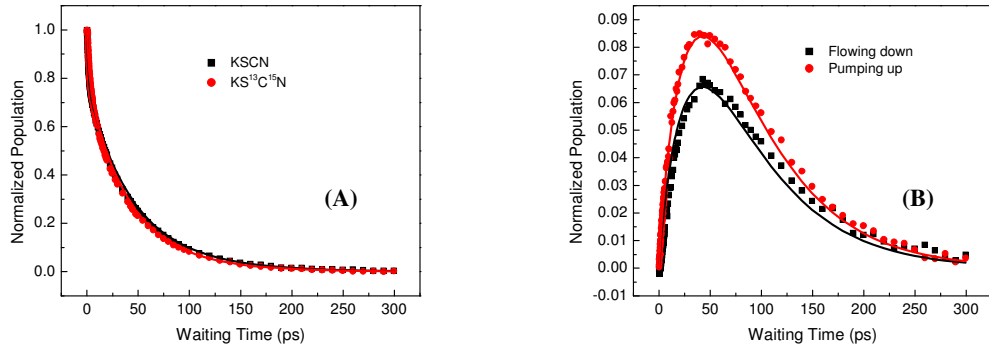


**Figure S4.** Data and calculations of nonresonance [(A) and (B)] for a 34%:66%  $\text{KS}^{13}\text{C}^{15}\text{N}/\text{KSCN}$  aqueous solution. Dots are data, and lines are calculations. Calculations for (A) and (B) are with input parameters:

$$\begin{aligned} k_{\text{clu}-\text{SCN}^{\sim}\text{fast}} &= 1/2.1 (\text{ps}^{-1}); k_{\text{clu}-\text{SCN}^{\sim}\text{slow}} = 1/63.0 (\text{ps}^{-1}); k_{\text{clu}-\text{S}^{13}\text{C}^{15}\text{N}^{\sim}\text{fast}} = 1/2.1 (\text{ps}^{-1}); k_{\text{clu}-\text{S}^{13}\text{C}^{15}\text{N}^{\sim}\text{slow}} = 1/68.0 (\text{ps}^{-1}); \\ k_{\text{iso}-\text{SCN}^{\sim}\text{fast}} &= 1/1.6 (\text{ps}^{-1}); k_{\text{iso}-\text{SCN}^{\sim}\text{slow}} = 1/28.0 (\text{ps}^{-1}); k_{\text{iso}-\text{S}^{13}\text{C}^{15}\text{N}^{\sim}\text{fast}} = 1/1.5 (\text{ps}^{-1}); k_{\text{iso}-\text{S}^{13}\text{C}^{15}\text{N}^{\sim}\text{slow}} = 1/22.0 (\text{ps}^{-1}); \\ k_{\text{clu} \rightarrow \text{iso}} &= 1/10.0 (\text{ps}^{-1}); K=40; k_{\text{SCN}^{\sim} \rightarrow \text{S}^{13}\text{C}^{15}\text{N}^{\sim}} = 1/143 (\text{ps}^{-1}); D=1.28 \end{aligned}$$

with pre-factors of the subgroups and offset of the bi-exponential

$$\begin{aligned} A_{\text{clu}-\text{SCN}^{\sim}\text{fast}} &= A_{\text{iso}-\text{SCN}^{\sim}\text{fast}} = 0.25; A_{\text{clu}-\text{SCN}^{\sim}\text{slow}} &= A_{\text{iso}-\text{SCN}^{\sim}\text{slow}} = 0.75; \\ A_{\text{clu}-\text{S}^{13}\text{C}^{15}\text{N}^{\sim}\text{fast}} &= A_{\text{iso}-\text{S}^{13}\text{C}^{15}\text{N}^{\sim}\text{fast}} = 0.21; A_{\text{clu}-\text{S}^{13}\text{C}^{15}\text{N}^{\sim}\text{slow}} &= A_{\text{iso}-\text{S}^{13}\text{C}^{15}\text{N}^{\sim}\text{slow}} = 0.79; \text{ offset} = 0 \end{aligned}$$

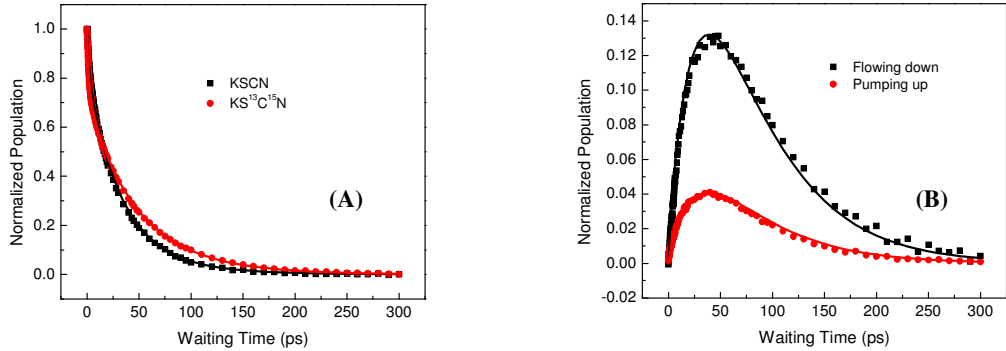


**Figure S5.** Data and calculations of nonresonance [(A) and (B)] for a 67%:33%  $KS^{13}C^{15}N/KSCN$  aqueous solution. Dots are data, and lines are calculations. Calculations for (A) and (B) are with input parameters:

$$\begin{aligned} k_{clu-SCN^- \text{ fast}} &= 1/2.4 (ps^{-1}); k_{clu-SCN^- \text{ slow}} = 1/60.0 (ps^{-1}); k_{clu-S^{13}C^{15}N^- \text{ fast}} = 1/2.1 (ps^{-1}); k_{clu-S^{13}C^{15}N^- \text{ slow}} = 1/66.0 (ps^{-1}); \\ k_{iso-SCN^- \text{ fast}} &= 1/1.8 (ps^{-1}); k_{iso-SCN^- \text{ slow}} = 1/21.0 (ps^{-1}); k_{iso-S^{13}C^{15}N^- \text{ fast}} = 1/1.3 (ps^{-1}); k_{iso-S^{13}C^{15}N^- \text{ slow}} = 1/24.0 (ps^{-1}); \\ k_{clu \rightarrow iso} &= 1/10.0 (ps^{-1}); K=40; k_{SCN^- \rightarrow S^{13}C^{15}N^-} = 1/68 (ps^{-1}); D=0.31 \end{aligned}$$

with pre-factors of the subgroups and offset of the bi-exponential

$$\begin{aligned} A_{clu-SCN^- \text{ fast}} &= A_{iso-SCN^- \text{ fast}} = 0.16; A_{clu-SCN^- \text{ slow}} = A_{iso-SCN^- \text{ slow}} = 0.84; \\ A_{clu-S^{13}C^{15}N^- \text{ fast}} &= A_{iso-S^{13}C^{15}N^- \text{ fast}} = 0.29; A_{clu-S^{13}C^{15}N^- \text{ slow}} = A_{iso-S^{13}C^{15}N^- \text{ slow}} = 0.71; \text{ offset} = 0 \end{aligned}$$

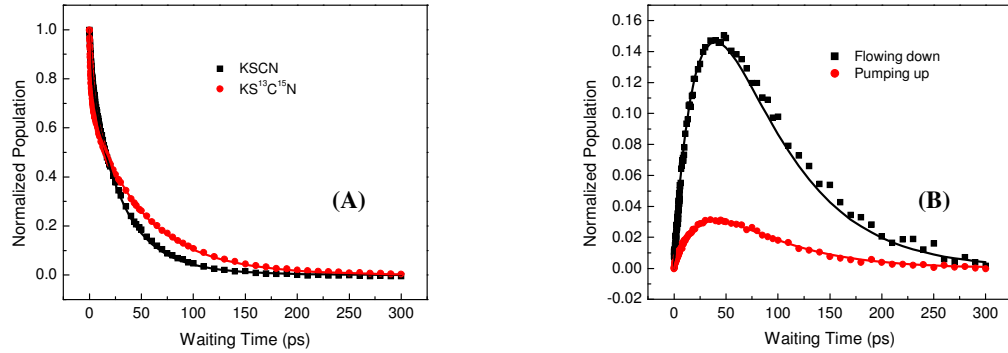


**Figure S6.** Data and calculations of nonresonance [(A) and (B)] for a 75%:25%  $KS^{13}C^{15}N/KSCN$  aqueous solution. Dots are data, and lines are calculations. Calculations for (A) and (B) are with input parameters:

$$\begin{aligned} k_{clu-SCN^- \text{ fast}} &= 1/2.1 (ps^{-1}); k_{clu-SCN^- \text{ slow}} = 1/64.0 (ps^{-1}); k_{clu-S^{13}C^{15}N^- \text{ fast}} = 1/1.2 (ps^{-1}); k_{clu-S^{13}C^{15}N^- \text{ slow}} = 1/64.0 (ps^{-1}); \\ k_{iso-SCN^- \text{ fast}} &= 1/1.9 (ps^{-1}); k_{iso-SCN^- \text{ slow}} = 1/20.0 (ps^{-1}); k_{iso-S^{13}C^{15}N^- \text{ fast}} = 1/1.1 (ps^{-1}); k_{iso-S^{13}C^{15}N^- \text{ slow}} = 1/28.0 (ps^{-1}); \\ k_{clu \rightarrow iso} &= 1/10.0 (ps^{-1}); K=40; k_{SCN^- \rightarrow S^{13}C^{15}N^-} = 1/56 (ps^{-1}); D=0.21 \end{aligned}$$

with pre-factors of the subgroups and offset of the bi-exponential

$$\begin{aligned} A_{clu-SCN^- \text{ fast}} &= A_{iso-SCN^- \text{ fast}} = 0.16; A_{clu-SCN^- \text{ slow}} = A_{iso-SCN^- \text{ slow}} = 0.84; \\ A_{clu-S^{13}C^{15}N^- \text{ fast}} &= A_{iso-S^{13}C^{15}N^- \text{ fast}} = 0.30; A_{clu-S^{13}C^{15}N^- \text{ slow}} = A_{iso-S^{13}C^{15}N^- \text{ slow}} = 0.70; \text{ offset} = 0 \end{aligned}$$

## Nonresonant energy transfer between $S^{13}C^{15}N^-$ and $SCN^-$ in 50%:50% $KS^{13}C^{15}N/KSCN$ crystal

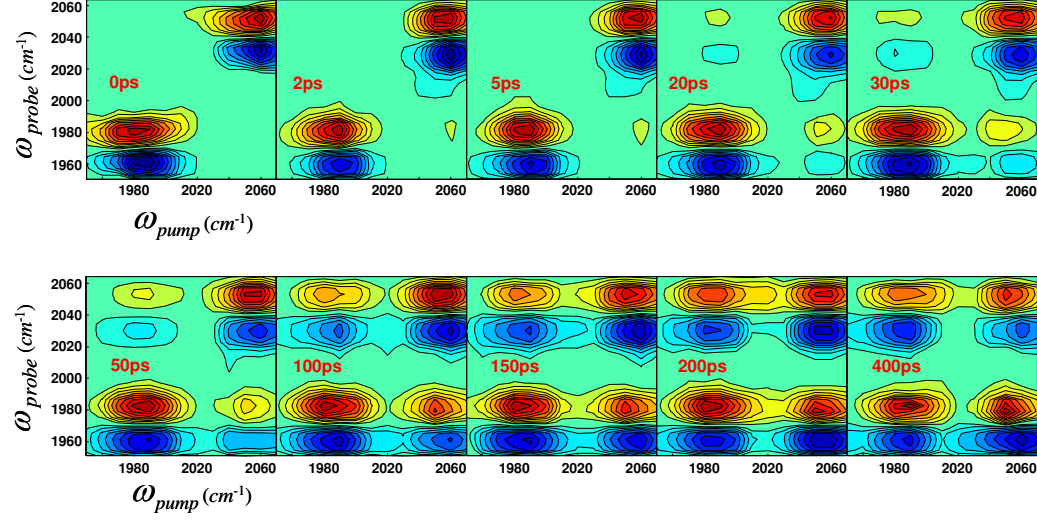
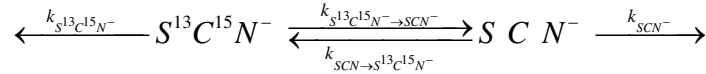


**Fig. S7.** 2D IR spectra of 50%:50%  $KS^{13}C^{15}N/KSCN$  crystal at different waiting times  $T_w$ . As  $T_w$  increases, the off-diagonal peaks grow in because of energy exchange between  $SCN^-$  and  $S^{13}C^{15}N^-$ .

Fig. S7 shows 2D IR spectra of 1:1 mixed  $KS^{13}C^{15}N/KSCN$  crystal at different waiting times at room temperature. It can be clearly observed that with the increase of the probe delay time, vibrational energy begins to flow between  $S^{13}C^{15}N^-$  and  $SCN^-$ . For the 1:1 mixed  $KS^{13}C^{15}N/KSCN$  crystal, we use a simple kinetic model which was described in previous literature<sup>4</sup> to analyze the nonresonant energy transfer between  $S^{13}C^{15}N^-$  and  $SCN^-$ .



In the model,  $SCN^-$  and  $S^{13}C^{15}N^-$  can exchange vibrational energy, and they also decay with their own vibrational lifetimes. Here the biexponential decay of the  $SCN^-$  stretch was used. The experimental results and the calculations with detailed input parameters are shown in Fig. S7.

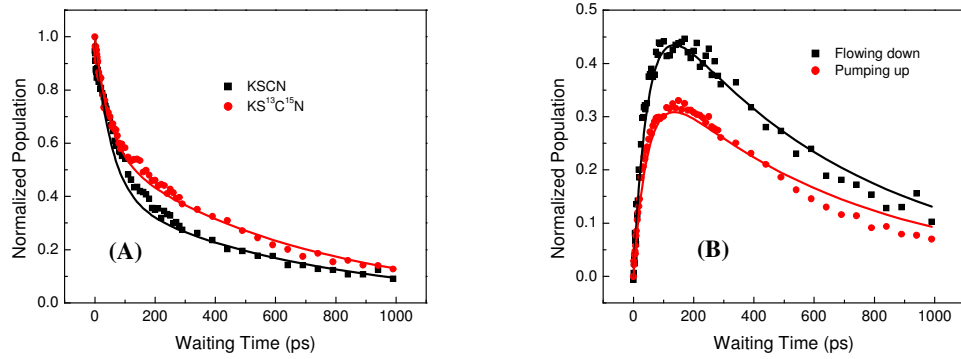


**Figure S8.** Data and calculations of nonresonance for a 50%:50%  $\text{KS}^{13}\text{C}^{15}\text{N}/\text{KSCN}$  crystal. Dots are data, and lines are calculations. Calculations for (A) and (B) are with input parameters:

$$k_{\text{SCN}^-\text{fast}} = 1/150 \text{ (ps}^{-1}\text{)}; k_{\text{SCN}^-\text{slow}} = 1/760 \text{ (ps}^{-1}\text{)}; k_{\text{S}^{13}\text{C}^{15}\text{N}^-\text{fast}} = 1/90 \text{ (ps}^{-1}\text{)}; k_{\text{S}^{13}\text{C}^{15}\text{N}^-\text{slow}} = 1/650 \text{ (ps}^{-1}\text{)};$$

$$k_{\text{SCN}^-\rightarrow\text{S}^{13}\text{C}^{15}\text{N}^-} = 1/103 \text{ (ps}^{-1}\text{)}; D=0.70$$

with pre-factors of the subgroups and offset of the bi-exponential

$$A_{\text{SCN}^-\text{fast}} = 0.02; A_{\text{SCN}^-\text{slow}} = 0.98; A_{\text{S}^{13}\text{C}^{15}\text{N}^-\text{fast}} = 0.03; A_{\text{S}^{13}\text{C}^{15}\text{N}^-\text{slow}} = 0.97; \text{offset} = 0.$$

## Rotations in KSCN/KS<sup>13</sup>C<sup>15</sup>N mixed crystals at room temperature

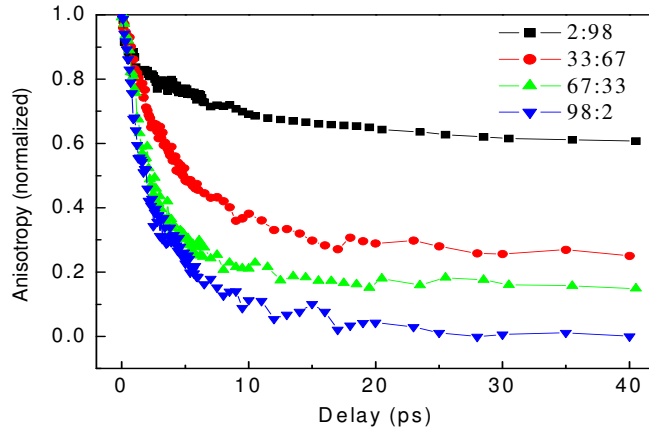


**Figure S9.** Anisotropy decay of the <sup>13</sup>C<sup>15</sup>N<sup>-</sup> stretch 1-2 transition pump/probe signal of S<sup>13</sup>C<sup>15</sup>N in KSCN/KS<sup>13</sup>C<sup>15</sup>N mixed crystals with different KSCN/KS<sup>13</sup>C<sup>15</sup>N molar ratios. The decay in the 2:98 sample is mainly caused by the anion wobbling around the equilibrium position. The decay in the 98:2 sample is mainly caused by the resonant energy transfer among the S<sup>13</sup>C<sup>15</sup>N<sup>-</sup> anions. Diluting S<sup>13</sup>C<sup>15</sup>N with SCN<sup>-</sup> can effectively reduce the number of resonant energy acceptors and therefore slow down the energy transfer induced anisotropy decay. The wobbling angle  $\theta_c$  can

be determined with the equation:  $\frac{r_\infty}{r_0} = \left[ \frac{1}{2} \cos \theta_c (1 + \cos \theta_c) \right]^2$ , where  $r_i$  is the anisotropy.

## Off-diagonal anharmonicity determination

At the earliest waiting time, when we pump SCN<sup>-</sup>, the cross peaks at the S<sup>13</sup>C<sup>15</sup>N<sup>-</sup> frequency position will appear. While the observed peak contains two contributions: (1) from direct pumping 1991 cm<sup>-1</sup> due to the small tail of the pump pulse, which produces peak pairs at probe frequencies of 1991 cm<sup>-1</sup>(positive) and 1967 cm<sup>-1</sup>(negative), and (2) from the coupling which also produces two peaks of 1991 cm<sup>-1</sup>(positive) and the combination band peak (negative). Based on the experimental result, the frequency of the negative coupling peak is determined by calculations summing up the two contributions with two adjustable parameters: the negative coupling frequency, the ratio of coupling positive peak to the direct pumping positive peak. The negative and positive coupling peak ratio is assumed to be 1. The negative and positive pumping peak ratio is determined by the diagonal peaks in 2D IR to be 0.8. The experimental data and the fitting results are given in Fig. S10 to S17.

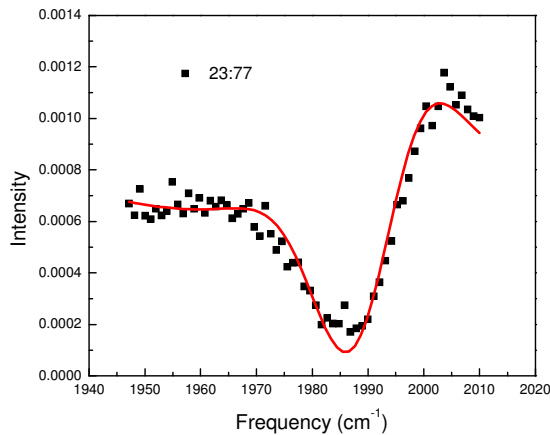


**Figure S10.** Experimental (dot) and calculated coupling peak (line) between SCN<sup>-</sup> and S<sup>13</sup>C<sup>15</sup>N<sup>-</sup> pumped at 2064 cm<sup>-1</sup>, probed at 1950~2010 cm<sup>-1</sup> for the 23%:77% KS<sup>13</sup>C<sup>15</sup>N/KSCN solution. The off-diagonal anharmonicity is  $\Delta_{SCN^-/S^{13}C^{15}N^-} = 2 \pm 2 \text{ cm}^{-1}$ .

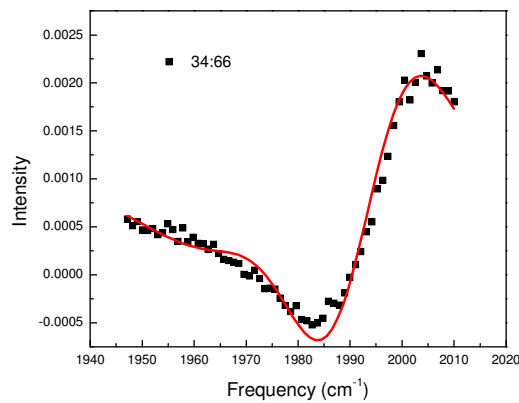


**Figure S11.** Experimental (dot) and calculated coupling peak (line) between SCN<sup>-</sup> and S<sup>13</sup>C<sup>15</sup>N<sup>-</sup> pumped at 2064 cm<sup>-1</sup>, probed at 1950~2010 cm<sup>-1</sup> for the 34%:66% KS<sup>13</sup>C<sup>15</sup>N/KSCN solution. The off-diagonal anharmonicity is  $\Delta_{SCN^-/S^{13}C^{15}N^-} = 3 \pm 2 \text{ cm}^{-1}$ .

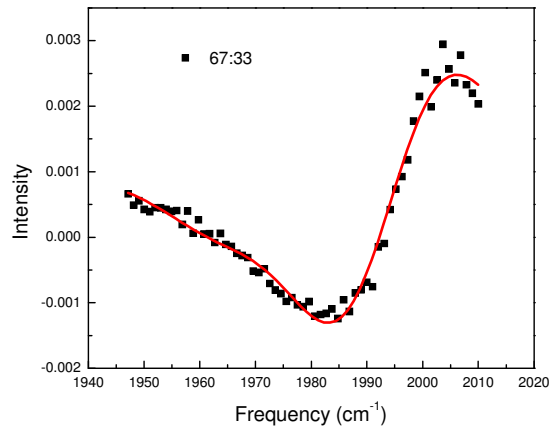


**Figure S12.** Experimental (dot) and calculated coupling peak (line) between SCN<sup>-</sup> and S<sup>13</sup>C<sup>15</sup>N<sup>-</sup> pumped at 2064 cm<sup>-1</sup>, probed at 1950~2010 cm<sup>-1</sup> for the 67%:33% KS<sup>13</sup>C<sup>15</sup>N/KSCN solution. The off-diagonal anharmonicity is  $\Delta_{SCN^-/S^{13}C^{15}N^-} = 6 \pm 2 \text{ cm}^{-1}$ .

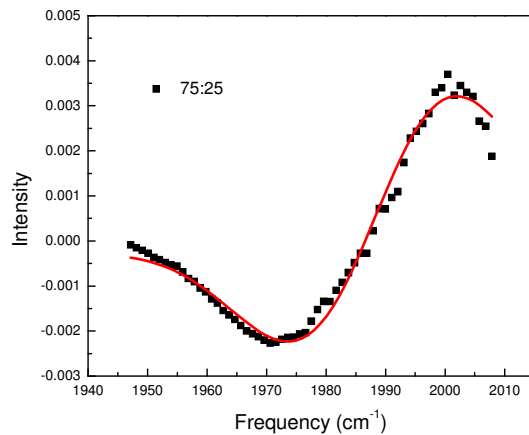


**Figure S13.** Experimental (dot) and calculated coupling peak (line) between SCN<sup>-</sup> and S<sup>13</sup>C<sup>15</sup>N<sup>-</sup> pumped at 2064 cm<sup>-1</sup>, probed at 1950~2010 cm<sup>-1</sup> for the 75%:25% KS<sup>13</sup>C<sup>15</sup>N/KSCN solution. The off-diagonal anharmonicity is  $\Delta_{SCN^-/S^{13}C^{15}N^-} = 8 \pm 3 \text{ cm}^{-1}$ .

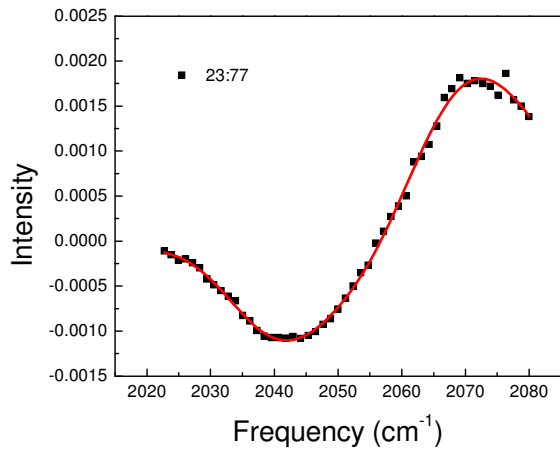


**Figure S14.** Experimental (dot) and calculated coupling peak (line) between SCN<sup>-</sup> and S<sup>13</sup>C<sup>15</sup>N<sup>-</sup> pumped at 1991 cm<sup>-1</sup>, probed at 2020~2080 cm<sup>-1</sup> for the 23%:77% KS<sup>13</sup>C<sup>15</sup>N/KSCN solution. The off-diagonal anharmonicity is  $\Delta_{\text{SCN}^-/\text{S}^{13}\text{C}^{15}\text{N}^-} = 7 \pm 3 \text{ cm}^{-1}$ .

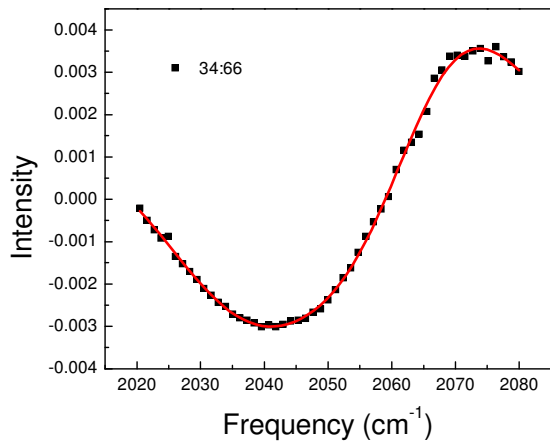


**Figure S15.** Experimental (dot) and calculated coupling peak (line) between SCN<sup>-</sup> and S<sup>13</sup>C<sup>15</sup>N<sup>-</sup> pumped at 1991 cm<sup>-1</sup>, probed at 2020~2080 cm<sup>-1</sup> for the 34%:66% KS<sup>13</sup>C<sup>15</sup>N/KSCN solution. The off-diagonal anharmonicity is  $\Delta_{\text{SCN}^-/\text{S}^{13}\text{C}^{15}\text{N}^-} = 5 \pm 2 \text{ cm}^{-1}$ .

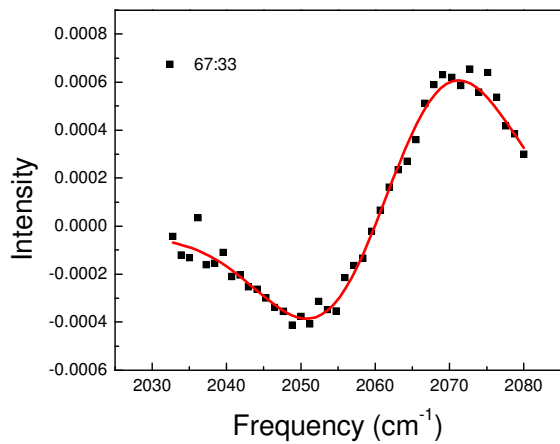


**Figure S16.** Experimental (dot) and calculated coupling peak (line) between SCN<sup>-</sup> and S<sup>13</sup>C<sup>15</sup>N<sup>-</sup> pumped at 1991 cm<sup>-1</sup>, probed at 2020~2080 cm<sup>-1</sup> for the 67%:33% KS<sup>13</sup>C<sup>15</sup>N/KSCN solution. The off-diagonal anharmonicity is  $\Delta_{SCN^-/S^{13}C^{15}N^-} = 3 \pm 2 \text{ cm}^{-1}$ .

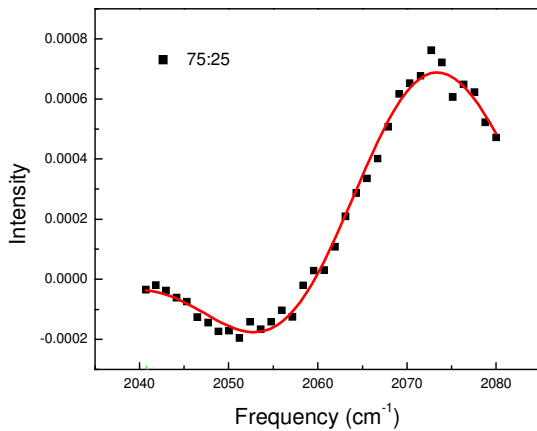


**Figure S17.** Experimental (dot) and calculated coupling peak (line) between SCN<sup>-</sup> and S<sup>13</sup>C<sup>15</sup>N<sup>-</sup> pumped at 1991 cm<sup>-1</sup>, probed at 2020~2080 cm<sup>-1</sup> for the 75%:25% KS<sup>13</sup>C<sup>15</sup>N/KSCN solution. The off-diagonal anharmonicity is  $\Delta_{SCN^-/S^{13}C^{15}N^-} = 2 \pm 2 \text{ cm}^{-1}$ .

## Coupling strength $\beta_{ij}$ determination

We can analytically get  $\beta_{ij}$  and other parameters in the local Hamiltonian H based on the known eigenstates and the diagonal and off-diagonal anharmonicity.<sup>4,8</sup> Through the diagonalization of the matrix H, the corresponding eigenvalues ( $\omega_k, \omega_l$ ) and the diagonal anharmonicities ( $\Delta_{kk}, \Delta_{ll}$ ) and off-diagonal anharmonicities ( $\Delta_{kl}$ ) can be reproduced using the best-fit values of the parameters in the local Hamiltonian. The results are listed in Table S1-S7.

**Table S1.** The input parameters and experimental data for the Hamiltonian matrix of SCN<sup>-</sup> and S<sup>13</sup>C<sup>15</sup>N<sup>-</sup> system with  $\Delta_{SCN^-/S^{13}C^{15}N^-} = 2 \pm 2 \text{ cm}^{-1}$  and  $\beta_{SCN^-/S^{13}C^{15}N^-} = 9.8 \pm 4.0 \text{ cm}^{-1}$ .

Input parameters	Experimental and diagonalization data
$\omega_i = 1992 \pm 1 \text{ cm}^{-1}$ , $\omega_j = 2063 \pm 1 \text{ cm}^{-1}$ $\beta_{ij} = 9.8 \pm 4.0 \text{ cm}^{-1}$ $\Delta_i = 25 \pm 1 \text{ cm}^{-1}$ , $\Delta_j = 25 \pm 1 \text{ cm}^{-1}$	$\omega_k = 1991 \text{ cm}^{-1}$ , $\omega_l = 2064 \text{ cm}^{-1}$ $\Delta_{kk} = 24 \text{ cm}^{-1}$ , $\Delta_{ll} = 24 \text{ cm}^{-1}$

**Table S2.** The input parameters and experimental data for the Hamiltonian matrix of SCN<sup>-</sup> and S<sup>13</sup>C<sup>15</sup>N<sup>-</sup> system with  $\Delta_{SCN^-/S^{13}C^{15}N^-} = 3 \pm 2 \text{ cm}^{-1}$  and  $\beta_{SCN^-/S^{13}C^{15}N^-} = 11.9 \pm 4.0 \text{ cm}^{-1}$ .

Input parameters	Experimental and diagonalization data
$\omega_i = 1993 \pm 1 \text{ cm}^{-1}$ , $\omega_j = 2062 \pm 1 \text{ cm}^{-1}$ $\beta_{ij} = 11.9 \pm 4.0 \text{ cm}^{-1}$ $\Delta_i = 25 \pm 1 \text{ cm}^{-1}$ , $\Delta_j = 26 \pm 1 \text{ cm}^{-1}$	$\omega_k = 1991 \text{ cm}^{-1}$ , $\omega_l = 2064 \text{ cm}^{-1}$ $\Delta_{kk} = 24 \text{ cm}^{-1}$ , $\Delta_{ll} = 24 \text{ cm}^{-1}$

**Table S3.** The input parameters and experimental data for the Hamiltonian matrix of SCN<sup>-</sup> and S<sup>13</sup>C<sup>15</sup>N<sup>-</sup> system with  $\Delta_{SCN^-/S^{13}C^{15}N^-} = 4 \pm 2 \text{ cm}^{-1}$  and  $\beta_{SCN^-/S^{13}C^{15}N^-} = 13.6 \pm 3.0 \text{ cm}^{-1}$ .

Input parameters	Experimental and diagonalization data
$\omega_i = 1993 \pm 1 \text{ cm}^{-1}$ , $\omega_j = 2062 \pm 1 \text{ cm}^{-1}$ $\beta_{ij} = 13.6 \pm 3.0 \text{ cm}^{-1}$ $\Delta_i = 25 \pm 1 \text{ cm}^{-1}$ , $\Delta_j = 27 \pm 1 \text{ cm}^{-1}$	$\omega_k = 1991 \text{ cm}^{-1}$ , $\omega_l = 2064 \text{ cm}^{-1}$ $\Delta_{kk} = 24 \text{ cm}^{-1}$ , $\Delta_{ll} = 24 \text{ cm}^{-1}$

**Table S4.** The input parameters and experimental data for the Hamiltonian matrix of SCN<sup>-</sup> and S<sup>13</sup>C<sup>15</sup>N<sup>-</sup> system with  $\Delta_{SCN^-/S^{13}C^{15}N^-} = 5 \pm 2 \text{ cm}^{-1}$  and  $\beta_{SCN^-/S^{13}C^{15}N^-} = 14.9 \pm 3.0 \text{ cm}^{-1}$ .

Input parameters	Experimental and diagonalization data
$\omega_i = 1993 \pm 1 \text{ cm}^{-1}$ , $\omega_j = 2062 \pm 1 \text{ cm}^{-1}$ $\beta_{ij} = 14.9 \pm 3.0 \text{ cm}^{-1}$ $\Delta_i = 26 \pm 1 \text{ cm}^{-1}$ , $\Delta_j = 27 \pm 1 \text{ cm}^{-1}$	$\omega_k = 1991 \text{ cm}^{-1}$ , $\omega_l = 2064 \text{ cm}^{-1}$ $\Delta_{kk} = 24 \text{ cm}^{-1}$ , $\Delta_{ll} = 24 \text{ cm}^{-1}$

**Table S5.** The input parameters and experimental data for the Hamiltonian matrix of SCN<sup>-</sup> and S<sup>13</sup>C<sup>15</sup>N<sup>-</sup> system with  $\Delta_{SCN^-/S^{13}C^{15}N^-} = 6 \pm 2 \text{ cm}^{-1}$  and  $\beta_{SCN^-/S^{13}C^{15}N^-} = 16.2 \pm 4.0 \text{ cm}^{-1}$ .

Input parameters	Experimental and diagonalization data
$\omega_i = 1995 \pm 1 \text{ cm}^{-1}$ , $\omega_j = 2060 \pm 1 \text{ cm}^{-1}$ $\beta_{ij} = 16.2 \pm 4.0 \text{ cm}^{-1}$ $\Delta_i = 26 \pm 1 \text{ cm}^{-1}$ , $\Delta_j = 28 \pm 1 \text{ cm}^{-1}$	$\omega_k = 1991 \text{ cm}^{-1}$ , $\omega_l = 2064 \text{ cm}^{-1}$ $\Delta_{kk} = 24 \text{ cm}^{-1}$ , $\Delta_{ll} = 24 \text{ cm}^{-1}$

**Table S6.** The input parameters and experimental data for the Hamiltonian matrix of SCN<sup>-</sup> and S<sup>13</sup>C<sup>15</sup>N<sup>-</sup> system with  $\Delta_{SCN^-/S^{13}C^{15}N^-} = 7 \pm 3 \text{ cm}^{-1}$  and  $\beta_{SCN^-/S^{13}C^{15}N^-} = 17.3 \pm 4.0 \text{ cm}^{-1}$ .

Input parameters	Experimental and diagonalization data
$\omega_i = 1996 \pm 1 \text{ cm}^{-1}$ , $\omega_j = 2059 \pm 1 \text{ cm}^{-1}$ $\beta_{ij} = 17.3 \pm 4.0 \text{ cm}^{-1}$ $\Delta_i = 26 \pm 1 \text{ cm}^{-1}$ , $\Delta_j = 29 \pm 1 \text{ cm}^{-1}$	$\omega_k = 1991 \text{ cm}^{-1}$ , $\omega_l = 2064 \text{ cm}^{-1}$ $\Delta_{kk} = 24 \text{ cm}^{-1}$ , $\Delta_{ll} = 24 \text{ cm}^{-1}$

**Table S7.** The input parameters and experimental data for the Hamiltonian matrix of SCN<sup>-</sup> and S<sup>13</sup>C<sup>15</sup>N<sup>-</sup> system with  $\Delta_{SCN^-/S^{13}C^{15}N^-} = 8 \pm 3 \text{ cm}^{-1}$  and  $\beta_{SCN^-/S^{13}C^{15}N^-} = 18.4 \pm 5.0 \text{ cm}^{-1}$ .

Input parameters	Experimental and diagonalization data
$\omega_i = 1996 \pm 1 \text{ cm}^{-1}$ , $\omega_j = 2059 \pm 1 \text{ cm}^{-1}$ $\beta_{ij} = 18.4 \pm 5.0 \text{ cm}^{-1}$ $\Delta_i = 27 \pm 1 \text{ cm}^{-1}$ , $\Delta_j = 29 \pm 1 \text{ cm}^{-1}$	$\omega_k = 1991 \text{ cm}^{-1}$ , $\omega_l = 2064 \text{ cm}^{-1}$ $\Delta_{kk} = 24 \text{ cm}^{-1}$ , $\Delta_{ll} = 24 \text{ cm}^{-1}$

## Derivation of the relation between the average coupling strength $\bar{V}$ and the one donor to one acceptor coupling strength $V_{12}$

We assume that there are  $n$  identical nonresonant acceptors in a cluster, and molecule “a” is initially excited.

We have the initial excited state

$$\Psi_i = \Psi_{a^*} \Psi_1 \Psi_2 \cdots \Psi_n,$$

and the final excited state

$$\Psi_f = \sqrt{\frac{1}{n}} (\Psi_a \Psi_{1^*} \cdots \Psi_n + \cdots + \Psi_a \Psi_1 \cdots \Psi_{n^*}).$$

The coupling (nonresonant) we measured is

$$\begin{aligned} \bar{V} &= \langle \Psi_i | V | \Psi_f \rangle = \sqrt{\frac{1}{n}} \langle \Psi_{a^*} \Psi_1 \Psi_2 \cdots \Psi_n | V | (\Psi_a \Psi_{1^*} \cdots \Psi_n + \cdots + \Psi_a \Psi_1 \cdots \Psi_{n^*}) \rangle \\ &= \sqrt{\frac{1}{n}} (\langle \Psi_a | V | \Psi_1 \rangle + \dots + \langle \Psi_a | V | \Psi_n \rangle) \\ &= \sqrt{\frac{1}{n}} (n \langle \Psi_a | V | \Psi_1 \rangle) \\ &= \sqrt{n} V_{12} \end{aligned}$$

### Reference

- (1) Bian, H. T.; Wen, X. W.; Li, J. B.; Chen, H. L.; Han, S.; Sun, X. Q.; Song, J.; Zhuang, W.; Zheng, J. R. *Proceedings of the National Academy of Sciences of the United States of America* 2011, **108**, 4737.
- (2) Zheng, J.; Kwac, K.; Xie, J.; Fayer, M. D. *Science* 2006, **313**, 1951.
- (3) Zheng, J. *Ultrafast Chemical Exchange Spectroscopy*; VDM Verlag, 2008.
- (4) Bian, H. T.; Wen, X. W.; Li, J. B.; Zheng, J. R. *J. Chem. Phys.* 2010, **133**, 034505.
- (5) Bian, H. T.; Li, J. B.; Wen, X. W.; Zheng, J. R. *J. Chem. Phys.* 2010, **132**, 184505.
- (6) Rey, R.; Hynes, J. T. *Journal of Chemical Physics* 1998, **108**, 142.
- (7) Merzbacher, E. *Quantum Mechanics.*, 3rd ed. ed.; John Wiley&Sons, Inc.: New York, 1998.
- (8) *Ultrafast Infrared and Raman Spectroscopy*; Fayer, M. D., Ed.; Marcel Dekker, Inc: New York, Basel, 2001; Vol. 26.